Brodogradnja Volume 78 Number 1 (2027) 78107

journal homepage: www.brodogradnja.fsb.hr

Brodogradnja

An International Journal of Naval Architecture and Ocean Engineering for Research and Development

Study on the effect of layout on navigation characteristics of trimaran in stern quartering seas

Jiaye Gong[1], *Yongle Jiang*[1], *Luyao Wang*[1], *Meng Wang*[2], *Zhichao Hong*[3,*]

[1]*College of Ocean Science and Engineering, Shanghai Maritime University, Shanghai, China*
[2]*School of Naval Architecture & Ocean Engineering, Jiangsu University of Science and Technology, Zhen-jiang, China*
[3]*School of Law, Shanghai University of International Business and Economics, Shanghai, China*

ARTICLE INFO

Keywords:
Trimaran
Layout
Surf-riding
Broaching
Motion response

ABSTRACT

As one of the high-performance ships, the performance of trimaran is significantly affected by the side hull position. The influence of side-hull positioning on the resistance and seakeeping of trimaran has been widely studied, but the effect on the sailing performance and broaching susceptibility is still not clear enough. In this paper, the autopilot of a trimaran model in waves is simulated by a hybrid method coupling Fully-nonlinear-potential-flow-theory (FNPT) and computational fluid dynamics (CFD), and the effect of the side hull position on the course keeping and broaching susceptibility is studied. The effect of the grid on the computed results is tested first. Then, the autopilot of the trimaran model with different layouts in quartering stern waves is simulated at a relatively high speed that could lead to broaching. By changing the wave steepness, the effect of the layout on the sailing performance and broaching of trimaran is studied. The research results indicate that the arrangement of the side hulls has a significant impact on the vessel's broaching phenomenon and course-keeping performance. Under steep wave conditions, a forward side-hull arrangement increases the vessel's susceptibility to broaching and weakens its course-keeping ability, while a rear side-hull arrangement with a larger transverse spacing demonstrates better directional stability and can effectively reduce the probability of broaching. The systematic analysis in this paper provides new insights for optimizing the stability of trimarans in following quartering seas.

1. Introduction

As a high-performance ship, trimaran has garnered widespread attention due to its exceptional speed, stability, and ample deck space. The design of a trimaran includes a main hull and two side bodies, a structure that provides stability and broaching damping while also presenting unique challenges in terms of wave response, especially the phenomenon of surf-riding and broaching that may occur in adverse sea conditions. Therefore, studying the motion characteristics of surf-riding and broaching in trimarans is crucial for their hull design and navigation. From the perspective of maritime regulations, although the second-generation intact stability criteria have not yet become mandatory at the International Maritime Organization (IMO), they

* Corresponding author.
E-mail address: hongzcjust@163.com

https://doi.org/10.21278/brod78107
Received 30 December 2025; Received in revised form 04 October 2026; Accepted 19 October 2026
Available online 09 November 2026
ISSN 0007-215X; eISSN 1845-5859

represent a significant breakthrough in the standardization of ship stability assessment. These criteria will be enforced as statutory provisions in the future, directly affecting ship design and construction through stricter anti-capsizing verification requirements, and providing a unified compliance basis for flag State administration and port State control, so as to implement navigation safety responsibilities at the legal level.

Surf-riding and broaching phenomena are one of the five stability failure modes defined by the International Maritime Organization (IMO) for the second-generation intact stability of ships [1]. In ship stability research, surf-riding generally refers to a state in which a ship, under the action of following or stern-quartering waves, attains a longitudinal speed close to the wave celerity and is captured by the wave, thereby moving synchronously or approximately synchronously with the wave. If surf-riding occurs when the ship is on the downslope section of a wave trough, it may further trigger broaching—a phenomenon in which the vessel suddenly loses steering control and yaws rapidly, with full rudder being unable to correct the course. This is accompanied by large heel angles, the yaw angle increases sharply, and in extreme cases, may lead to capsizing. Optimizing the side hull layout of a trimaran (the longitudinal and transverse positions of the side hulls) can effectively regulate the vessel's motion response characteristics, thereby reducing the likelihood of instability phenomena such as surf-riding and broaching, and providing a reference for the stability design of trimarans.

In recent years, scholars have conducted extensive research on the hydrodynamic performance of trimarans, particularly in terms of resistance [2, 3], propulsion [4, 5], maneuvering [6-8], and seakeeping performance [9, 10]. The navigation characteristics of trimarans in following seas and stern quartering seas are an important for the seakeeping performance and form the basis for the safety and stability in waves. Methods for studying the motion characteristics of trimarans in waves mainly include tank test and numerical simulation. With the development of computer technology, CFD methods have been widely applied in the motion response of ship in waves. Begovic et al. [11] used OpenFOAM software for CFD simulation of the probability of motion in waves for the D-series ship type and analyzed the differences between single-degree-of-freedom and three-degree-of-freedom motion models. Gong et al. [12, 13] developed a hybrid algorithm to study the dynamic response of trimarans in waves, combining CFD for internal viscous flow and QALE-FEM external flow field simulation based on the FNPT method, and conducted an in-depth analysis of surf-riding and broaching behavior under different wave conditions and speeds. Liu et al. [14, 15] used URANS solvers and dynamic overlapping grid technology to study the relationship between surf-riding, loss of stability, broaching, and capsizing, with a particular focus on the impact of wave forces on ship stability. Ma et al. [16] used CFD methods to simulate the maneuvering hydrodynamic forces of the S175 container ship in waves and discussed the relationship between the course stability in waves and broaching. Zhou et al. [17] evaluated the hydrodynamic performance of a trimaran advancing in finite water depth, fully considering the coupling effects between steady and unsteady flows. The wave-making resistance of the trimaran increases significantly in shallow water, and the peak resistance rises as the water depth decreases. Both hull arrangement and water depth affect the motions, resistance, and seakeeping performance of the trimaran. Jeong et al. [18] focused on a hybrid numerical framework and data-driven strategies, which improved the accuracy of evaluating wave-induced motions and stability failures.

Although a large number of studies have explored the effects of trimaran hull configurations on broaching, yawing, and ship motions, existing research on the longitudinal arrangement of outriggers has mostly focused on configurations in which the outriggers are positioned forward of midship. Such configurations can significantly reduce roll, pitch, and heave responses under both regular and irregular waves. Increasing the transverse spacing between the main hull and the outriggers can effectively improve "transverse stability" and reduce the probability of broaching. However, the mechanisms by which different outrigger arrangements affect the seakeeping performance and susceptibility to broaching of trimarans in following seas and stern-quartering seas remain unclear. In view of the shortcomings of previous studies on trimaran configurations and ship stability in following seas and stern-quartering seas, this paper investigates the close relationship between trimaran configuration design and the risk of instability under severe sea conditions, as well as the influence of hull configuration on course stability and broaching instability. This study aims to analyze the effects of layout on the course stability, broaching phenomena, and corresponding motions of

trimarans. First, a hybrid method combining FNPT and CFD is used to conduct numerical simulations of an autopiloted trimaran under following-sea and stern-quartering-sea conditions, with the simulation process taking into account nonlinear motions, outrigger emergence, and bow diving phenomena. Subsequently, the layout is modified by moving the outriggers forward and increasing the spacing between the hulls, thereby investigating the influence of layout on the ship's wave-motion responses, with particular emphasis on its effects on course stability and the occurrence of broaching phenomena. However, the present study mainly focuses on the motion responses, course-keeping performance, and susceptibility to broaching of the trimaran. Although the broaching criterion is introduced in the paper, the occurrence time, duration, probability of occurrence, and critical conditions of broaching are not systematically quantified. Therefore, the conclusions regarding broaching in this paper can only be regarded as preliminary results under specific operating conditions. In particular, the ranges of instability speeds and wavelengths identified in this paper under limited conditions of initial speed, wave steepness, wavelength, and wave direction cannot be regarded as general critical conditions for broaching or yawing applicable to different ship types and sea states.

2. Numerical methods

In this section, an overview of the numerical approach employed for simulating the autopilot-equipped trimaran is initially provided.

2.1 Fundamental equations

For an accurate depiction of broaching behaviors of trimaran, it is imperative to consider the nonlinear phenomena, such as the side hull emergence above the water and bow diving. To capture these nuances, the simulation employs a viscous flow method to analyze the flow in the immediate vicinity of the trimaran. The governing equations for this incompressible flow are encapsulated by the Unsteady Reynolds-Averaged Navier-Stokes (URANS) equations as follows:

$$\nabla\cdot\boldsymbol{U}=0 \tag{1}$$

$$\frac{\partial(\rho\boldsymbol{U})}{\partial t}+\nabla\cdot\left[\rho(\boldsymbol{U}-\boldsymbol{U}_g)\boldsymbol{U}\right]=-\nabla p_d-\boldsymbol{g}\cdot\boldsymbol{x}\nabla\rho+\nabla\cdot(\mu_{eff}\nabla\boldsymbol{U})+(\nabla\boldsymbol{U})\cdot\nabla\mu_{eff}+f_\sigma+f_s \tag{2}$$

where ρ represents density, t represents time, g represents the gravitational acceleration, $\boldsymbol{U}=(u, v, w)$ in Cartesian coordinates represents the fluid velocity components, $\boldsymbol{U}_g$ represents the grid's motion velocity, p_d represents the dynamic pressure field, $\boldsymbol{g}\cdot\boldsymbol{x}\nabla\rho$ denotes the gravitational potential energy gradient term, μ_{eff} represents the effective dynamic viscosity, f_σ represents the surface tension term, f_s represents the source term. The VOF method, combined with compression techniques, is utilized to model the Eulerian two-phase flow of air and water. An artificial compression method, as detailed by [19, 20], is integrated into OpenFOAM to maintain a continuous and non-zero value at the air-water interface.

The governing equation and the associated boundary conditions for the fully nonlinear potential flow are written in terms of the velocity potential ϕ as:

$$\nabla^2\phi = 0 \quad \text{in the fluid domain} \tag{3}$$

$$\frac{\partial\phi}{\partial n}=\boldsymbol{n}\cdot\boldsymbol{U} \quad \text{on the wavemaker} \tag{4}$$

$$\frac{\partial\phi}{\partial n}=0 \quad \text{on the right, left and bottom} \tag{5}$$

$$\frac{D\boldsymbol{r}}{Dt}=\nabla\phi \quad \frac{D\phi}{Dt}=-gz+\frac{1}{2}|\nabla\phi|^2 \quad \text{on the free surface} \tag{6}$$

where $\boldsymbol{r}$ is the position vector of the free surface, $\boldsymbol{U}$ and $\boldsymbol{n}$ are the velocity and normal vector of the wavemaker boundary, t is time, D/Dt is the total time derivative, g is the gravitational acceleration, and z is the vertical coordinate in the spatial coordinate system. On the wavemaker, the self-correction wave generation mechanism is employed to generate waves, while the localized self-adaptive wave absorber is applied on the wave absorber boundary to reduce the wave reflection. As will being discussed in the following subsection, the trimarans are not included in the QALE-FEM domain and, thus, the boundary conditions on the trimaran surface are not needed.

The hybrid method combining the QALE-FEM method based on a fully nonlinear potential flow theory in the external field with the internal field viscous flow calculation domain is used in this paper. When the trimaran sails in waves, the internal region, including the ship, moves together with the ship within a larger external region. The internal domain is a NS viscous flow domain, which uses an incompressible unsteady Navier-Stokes (NS) model to simulate the motion of the trimaran in waves. The external domain is assumed to be an ideal fluid, and the generation of waves is simulated based on the fully nonlinear potential flow theory, where the velocity potential satisfies the Laplace equation. A wave maker is placed on one boundary of the external domain to generate waves, while an adaptive wave absorber is used on the other side to reduce wave reflection. The free surface simultaneously meets kinematic and dynamic boundary conditions. Figure 2 shows the two domains of the hybrid method, and Figure 1 is a simulation flowchart of the hybrid method. Table 1 compares the general CFD methods with the hybrid method. Given the extensive use of hybrid methods in Fluid-Structure Interaction (FSI) problems, further insights into the QALE-FEM and hybrid techniques can be gleaned from the cited literature [21-24]. These references provide a comprehensive overview of the methodologies applied to address various aspects of FSI.

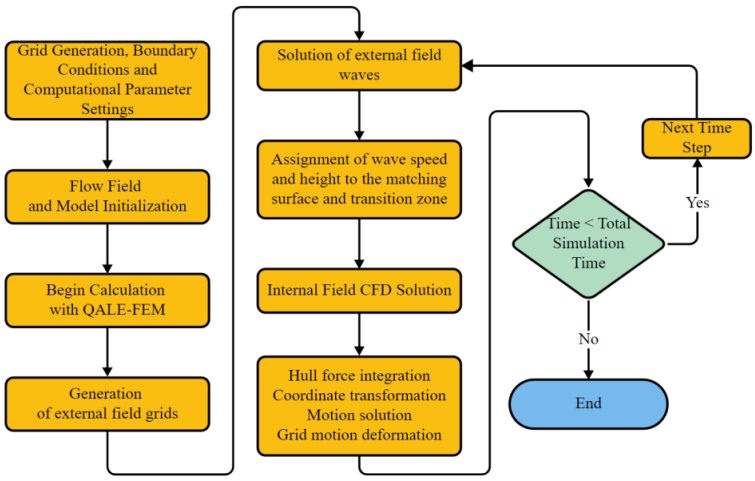


Fig. 1 Flow chart of the QaleFOAM

Table 1 Comparison between Hybrid Method and General CFD Method

Aspect	QALEFOAM	General CFD Methods
Approach	Hybrid method combining FNPT-based QALE-FEM with viscous flow methods.	Purely viscous flow-based simulations using Navier-Stokes equations without external domain coupling.
External Domain	Simulates wave dynamics using FNPT (Fully Nonlinear Potential Theory) for calm water and waves.	Not typically included; simulation is restricted to viscous flow within the computational domain.
Internal Domain	Uses viscous flow methods with unsteady incompressible Navier-Stokes equations for ship maneuvering.	Solely relies on viscous flow without coupling to an external potential flow model.
Grid and Boundary Handling	Employs a hybrid approach with transition zones connecting external and internal domains.	Uniform computational domain; grids are refined near areas of interest, but no coupling with external potential flow domains.
Wave-Ship Interaction	Considers nonlinear interactions, including wave slamming, green water, and intermittent hull emergence.	Simulates wave-ship interaction under the Navier-Stokes equations.
Computation Scope	Captures both external wave field and internal ship motion fields.	Focused solely on internal flow fields; may require higher computational resources for comparable detail in wave effects.
Application Examples	Suitable for high-fidelity analysis of ships in complex wave environments, e.g., zigzag and turning maneuvers in waves.	Broad application in general hydrodynamics.

2.2 Motion of the autopilot trimaran

In this paper, a local coordinate system o'-$x'y'z'$ is utilized to determine the trimaran motion. The origin of this local coordinate system is established at the gravity center trimaran, with the x' axis directed towards the bow and the y' axis towards the starboard side. The local coordinate system maintains a fixed position relative to the ship. The trimaran is allowed to navigate freely, and the simulation accounts for movements in heave, sway, surge, roll, pitch, and yaw. The equations that are used to solve for the trimaran motion are presented subsequently.

$$m(\dot{u}_{x'}-u_{y'}r_{z'}+u_{z'}r_{y'})=F_{Hx'}+F_{WJx'} \tag{7}$$

$$I_{x'}\dot{r}_{x'}+(I_{z'}-I_{y'})r_{y'}r_{z'}=M_{Hx'}+M_{WJx'} \tag{8}$$

where, m is the trimaran mass, translational motion (Taking the x' direction as an example, the same applies to the y' and z' directions) in the local coordinate system is represented by velocities ($u_{x'}$) and their corresponding accelerations, rotational motion (Taking the x' direction as an example, the same applies to the y' and z' directions) is denoted by angular velocities ($r_{x'}$) and their corresponding angular accelerations. The hydrodynamic forces and moments ($F_{Hx'}$) and ($M_{Hx'}$) are obtained from the solution of the internal viscous flow domain at each time step, ($F_{WJx'}$) and ($M_{WJx'}$) represent the jet propulsion forces and moments, respectively. The moments of inertia are given by ($I_{x'}$), which is obtain by a semi-empirical model [25-27]. At the initial stage of the simulation, the total thrust of the water jets is equivalent to the drag in still water. Subsequently, as the nozzle deflection controls the yawing of the trimaran, the thrust and steering forces of the water jets are derived through the conservation of momentum. The rotational motion is characterized by the Euler angles (ξ_4, ξ_5, ξ_6). Once Equation (9) has been solved, and the rates of change of these Euler angles are determined, which describe the rotation progression. This method allows for the quantification of the trimaran rotational dynamics.

$$\begin{bmatrix} \dot{\xi}_4 \\ \dot{\xi}_5 \\ \dot{\xi}_6 \end{bmatrix} = \begin{bmatrix} 1 & \sin\xi_4\tan\xi_5 & \cos\xi_4\tan\xi_5 \\ 0 & \cos\xi_4 & -\sin\xi_4 \\ 0 & \sin\xi_4/\cos\xi_5 & \cos\xi_4/\cos\xi_5 \end{bmatrix} \begin{bmatrix} r_{x'} \\ r_{y'} \\ r_{z'} \end{bmatrix} \tag{9}$$

A proportional-derivative (PD) autopilot was implemented with an initial heading of 0° set as the reference point. The yaw angle ξ_6 serves as the discrepancy at each time interval, and the associated angular velocity $\dot{\xi}_6$ represents the rate at which this discrepancy changes. Consequently, the desired nozzle deflection angle is computed at each time step using the formula $\delta=K_p\xi_6+K_d\dot{\xi}_6$, where K_p=9.5, K_d=3.0. The significant role of the differential gain (K_d) in suppressing subharmonic yaw motions for a trimaran in following seas, as highlighted by [28], was considered in our parameter selection. The chosen value of K_d=3.0 aims to provide sufficient damping to achieve stable course-keeping, consistent with their findings. For the simulation of the autopilot, values of δ_{max}=35° and a rate of change $\dot{\delta}$=10°/s are adopted. This implies that the nozzle deflection angle will adjust from its current value towards the target at a rate of 10°/s at each time step, facilitating the autopilot response to the trimaran yawing motion.

In the NS model, the two-phase incompressible NS model is employed and summarized below for the corresponding ALE form:

$$\frac{\partial(\rho u)}{\partial x}+\frac{\partial(\rho v)}{\partial y}+\frac{\partial(\rho w)}{\partial z}=0 \tag{10}$$

$$\frac{\partial(\rho u)}{\partial t}+\nabla\cdot\left[\rho(u-u_g)\boldsymbol{U}_f\right]=\nabla\cdot\left(\mu\nabla u\right)-\frac{\partial p_d}{\partial x}+f_x \tag{11}$$

$$\frac{\partial(\rho v)}{\partial t}+\nabla\cdot\left[\rho(v-v_g)\boldsymbol{U}_f\right]=\nabla\cdot\left(\mu\nabla v\right)-\frac{\partial p_d}{\partial y}+f_y \tag{12}$$

$$\frac{\partial(\rho w)}{\partial t}+\nabla\cdot\left[\rho(w-w_g)\boldsymbol{U}_f\right]=\nabla\cdot\left(\mu\nabla w\right)-\frac{\partial p_d}{\partial z}+f_z \tag{13}$$

where ρ is fluid density, $\boldsymbol{U}_f$ = (u, v, w) is the fluid velocity and $\boldsymbol{U}_g$=(u_g, v_g, w_g) is the velocity of the computational grid, p_d is the dynamic pressure, (f_x,f_y,f_z) represents external body force and, $f_z=-\rho g$ in this paper. The grid moves using the dynamic mesh technique to conform to the motion of the trimaran.

2.3 Domain and grid generation

In this paper, the dimensions of the internal domain are 4.5L×3.0L×2.0L in the longitudinal, transverse, and vertical directions, respectively. The lengths of the water above and below the surface are 0.5L and 1.0L, respectively. The internal domain mesh is generated using preprocessing tools blockMesh and snappyHexMesh of OpenFOAM. The mesh generation are similar to those used in the simulation of the trimaran maneuvering in waves as described in [29, 30]. The boundary definitions and a schematic of the grid for the hybrid method are illustrated in Figure 2.

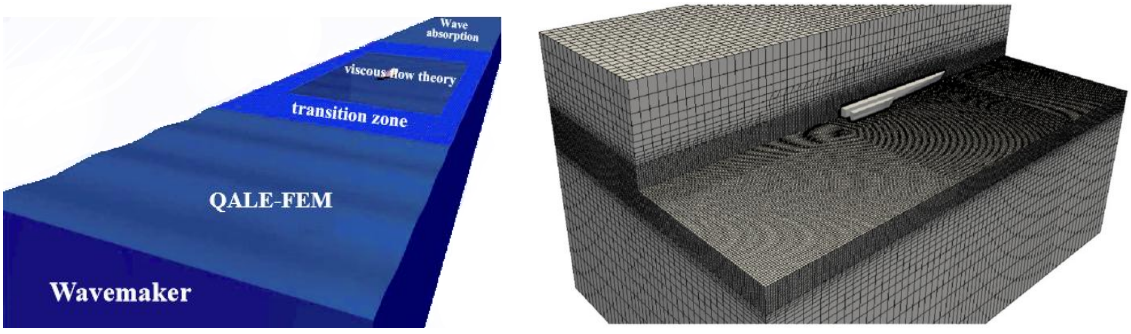


Fig. 2 The sketch of the hybrid method's boundary and the internal domain's grid

Within the scope of this study, the k-ω SST model has been selected to characterize turbulence. The PISO algorithm, which stands for pressure implicit with splitting of operators, is employed to address the interdependent nature of pressure and velocity fields. Further specifics regarding the boundary conditions of the internal domain are presented in Figure 3. It is important to highlight that the interface's velocity and volume fraction are dictated by the external domain, which is based on the FNPT method. This external domain is resolved prior to the internal domain at each time step, following the procedure outlined by [31].

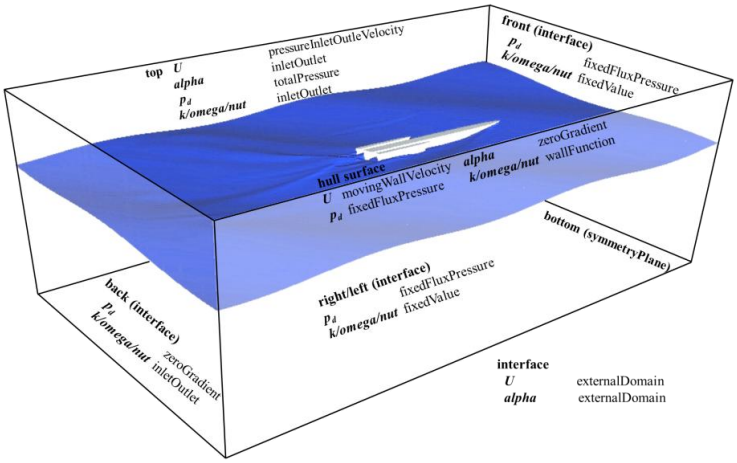


Fig. 3 The sketch of boundary condition and the grid

3. Verification Study

The hybrid numerical method adopted in the present study has been validated in previous studies. These studies include the turning and zigzag maneuvering tests of a trimaran and the KVLCC2 in both calm water and waves [12, 30], ship motion experiments in waves [13], and wave generation and propagation tests [29]. In these studies, the numerical predictions were compared with the corresponding experimental measurements, demonstrating the applicability of the hybrid method to ship maneuvering, wave-induced motions, and nonlinear wave simulations. Since the experimental validation of the hybrid numerical method has already been completed in the aforementioned studies, it is not repeated in the present work. Therefore, this section focuses on a grid-convergence analysis to evaluate the influence of mesh resolution on the predicted sailing trajectory and heading response. Numerical simulations are conducted using the trimaran model with three different layouts, which are formed by altering the hull separation and the longitudinal positions of the side hulls.

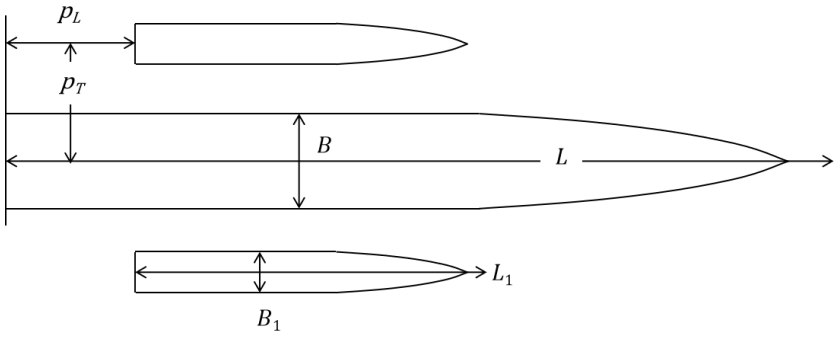


Fig. 4 The sketch of a trimaran and the dimensions

A sketch of the trimaran form is shown in Figure 4. The characteristic dimension of the trimaran for test is as follows: B/L=0.08, D/L=0.04, C_b=0.52, B_1/L_1=0.05, D_1/L_1=0.04, C_{b1}=0.46, p_t/L=0.1, p_L/L=0.3, where L, B, D are the waterline length, waterline width, draft of the center hull, L_1, B_1, and D_1 are the parameters of the side hull, C_b and C_{b1} are the block coefficient of the center hull and side hull, p_L and p_t are the longitudinal and transverse positions of the side hulls as shown in Figure 4. The wavelength λ/L=1.1, wave steepness of

ak=0.058, 0.096, 0.135, initial speed *Fr*=0.45, and initial wave heading β=30° are used for the test. The ratio $\sqrt{2}$ is used as the grid refinement. The cell numbers of coarse, medium, and fine mesh are 1.04×10^6, 2.67×10^6, and 6.83×10^6.

As shown in Figure 5, the difference lead by the mesh gets more noticeable when the wave steepness increases, and the motion trend by the coarse mesh is obviously different from that by medium and fine mesh in steep waves. For Figures 5(a)(b) and 5(c)(d), it shows that the roll and pitch motion of the trimaran is more sensitive to grid refinement than the trajectory and heading control. It is more evident from Figure 5(c) that the sensitivity of coarse, medium, and fine meshes to the rolling motion varies significantly over time. Under *ak*=0.058, rolling amplitudes by three meshes peak almost simultaneously at 22s with 6-8°; when *ak*=0.135, the difference between three meshes is relatively more obvious after 8s. Based on ITTC recommendation [32], the uncertainty analysis is conducted. For this purpose, the first order Richardson extrapolation δ^*_{REG4}, accuracy order p_G, correction factor C_G and grid uncertainty U_G are calculated by

$$\delta^*_{RE_{G4}} = \left(\frac{\varepsilon_{G21}}{r_G^{p_G}-1}\right) \tag{14}$$

$$p_G = \frac{\ln[(\varepsilon_{G32})/(\varepsilon_{G21})]}{\ln r_G} \tag{15}$$

$$C_G = \frac{r_G^{p_G}-1}{r_G^{p_{G_{est}}}-1} \tag{16}$$

$$U_G = \left|C_G\delta^*_{RE_{G4}}\right| + \left|(1-C_G)\delta^*_{RE_{G4}}\right| \tag{17}$$

where grid refinement ratio is $r_G = \sqrt{2}$, $p_{G_{est}} = 2$ is used in Equation (14), $\varepsilon_{Gij} = f_{G_i} - f_{G_j}$ is the difference between f_{G_i} and f_{G_j}, which are the computed result by using Grid G_i. Take the time broaching occurs to test the uncertainty, and it can be seen that when ak=0.058, no broaching occurs in the coarse, medium, and fine meshes. When ak=0.096, all three meshes experience one broaching event, with the coarse mesh occurring at 6.236 s, the medium mesh at 6.097 s, and the fine mesh at 6.086 s. When ak=0.135, the coarse mesh does not experience broaching, while the medium mesh experiences one event at 7.547s and the fine mesh at 7.304 s. Based on the GCI method [32], the uncertainty when ak=0.096 is about UG=6.379 %. Hence, the medium mesh can provide relatively accurate results at a lower computational cost. For the study effectiveness, the medium mesh is used for simulation hereafter. The accuracy orders of the relevant calculation results are shown in Table 2. The time discretization uses a first-order Euler scheme with a theoretical time accuracy of first order. The specific solution time step is Δt=0.015 s. The internal viscous flow field adopts the k-ω SST turbulence model.

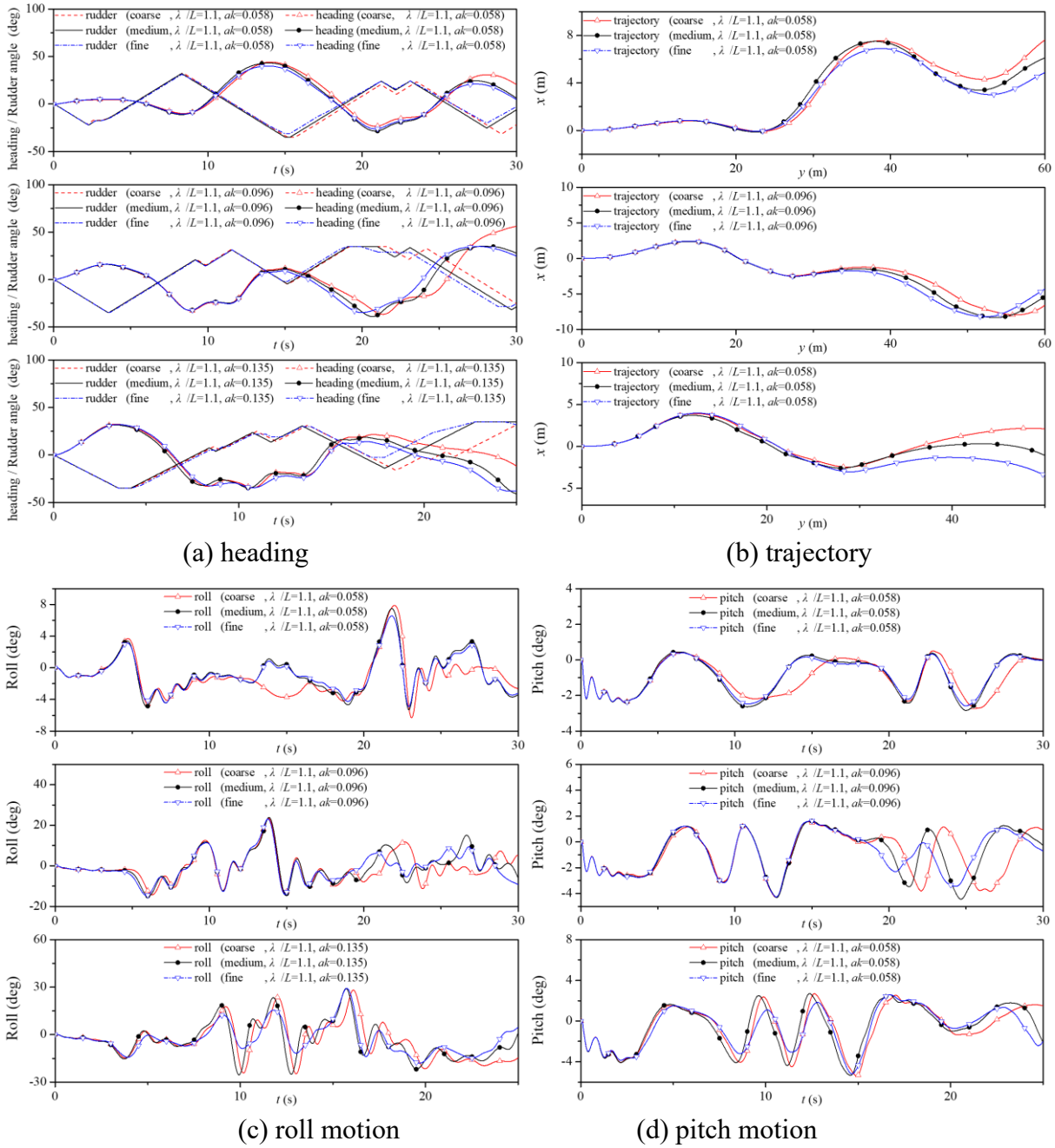


Fig. 5 The computed results by different mesh schemes for trimaran with side hull amidship

Table 2 Grid convergence analysis of the occurrence time of broaching under different wave steepnesses

ak	f_{G_3} coarse/s	f_{G_2} medium/s	f_{G_1} fine/s	ε_{G21}/s	ε_{G32}/s	P_G	Richardson extrapolation/s
0.058	NO broaching	NO broaching	NO broaching	N/A	N/A	N/A	N/A
0.096	6.236	6.097	6.086	0.011	0.139	3.660	6.085
0.135	NO broaching	7.547	7.304	N/A	N/A	N/A	N/A

G_1、G_2 and G_3 denote the fine, medium, and coarse meshes, respectively. f_{G_3} coarse/s denotes the broaching occurrence time predicted using the coarse mesh, in seconds; f_{G_2} medium/s and f_{G_1} fine/s denote the corresponding values for the medium and fine meshes, respectively. ε_{G21}/s is the absolute difference between the medium- and fine-mesh results, while ε_{G32}/s is the absolute difference between the coarse- and medium-mesh results. P_G denotes the calculated apparent order of convergence based on the results from the three meshes. Richardson extrapolation/s denotes the Richardson-extrapolated value, representing the theoretical result as the mesh size approaches zero. "No broaching" indicates that no time satisfying the broaching criterion was detected. "N/A" indicates that the parameter is not applicable because the required broaching-time data were unavailable.

4. Results and discussions

This section conducts a simulation analysis on the broaching phenomenon of an autopilot trimaran in following oblique seas. The impact of three different side-hull position on the motion response is discussed.

4.1 The impact of layout on instability

In most existing trimaran designs, the longitudinal position of the side hulls is generally arranged in the mid-aft or stern region of the main hull. For example, the side hulls of the British RV Triton trimaran experimental vessel are located near the middle of the main hull, while the side hulls of the American LSC trimaran are arranged at the rear of the main hull. According to existing publicly available literature, no representative full-scale trimaran has been found with side hulls arranged forward of the middle of the main hull. Therefore, this paper selects two side hull longitudinal arrangement schemes, namely, the middle and stern of the main hull, for investigation, and the longitudinal coordinate axis is arranged along the centerline of the main hull, with the coordinate origin set at the aft perpendicular of the main hull and the positive coordinate direction pointing toward the bow. The transverse separation of the side hulls usually ranges from $0.05L$ to $0.15L$, and two values of $0.1L$ and $0.15L$ are adopted in this study. The three side-hull layout schemes are listed in Table 3.

Table 3 Side-hull configurations considered in the present study

Layout	Transverse spacing	Longitudinal positions
Layout1	p_T/L=0.10	p_L/L=0.0
Layout2	p_T/L=0.15	p_L/L=0.0
Layout3	p_T/L=0.10	p_L/L=0.3

During navigation, the motion characteristics of trimarans are also affected by wave and navigation parameters, such as wavelength and wave steepness, speed and heading. When a trimaran is sailing in following waves, higher wave steepness tends to result in more intense surging and rolling at the wave crests, which may trigger surf-riding and lead to instable motion response [21]. In steep waves, the leeward hull piercing into the wave face or trough during rolling will trigger a "tripping" fulcrum effect, which drastically reduce stability and cause capsize [33, 34]. With the force acting deep beneath the bow, a powerful lever effect intensifies rolling, which lifts the stern, inducing side-swing or even broaching [35]. Therefore, the initial

Froude number Fr is fixed at 0.45 for all cases, which is of high-risk to trigger surf-riding and broaching [13]. Firstly, the wavelengths to waterline length ratio λ/L from 0.9 to 1.7 with wave steepness ak=0.096 is simulated. Then, the simulation with ak=0.14 is conducted, with λ/L increasing from 0.5 to 2.1. Detailed information of the working conditions is shown in Tables 4 and 5. However, in investigating the effects of wavelength and wave steepness, this study fixed the initial Froude number at Fr=0.45. Therefore, within the parameter range examined, the individual effects and coupled influences of the initial ship speed, wavelength, wave steepness, and incident wave direction angle on broaching and yawing have not yet been fully distinguished. In particular, the effects of wavelength and wave steepness were analyzed under fixed initial speed and wave direction angle conditions. Therefore, the selected Fr=0.45 represents only an operating condition with a relatively high risk of instability and should not be regarded as a universal critical speed for the broaching phenomenon.

Table 4 Working condition with ak=0.096

λ/L	Fr	ak	β	Layout
0.9	0.45	0.096	0°	
1.1				Layout1
1.3				Layout2
1.5				Layout3
1.7				

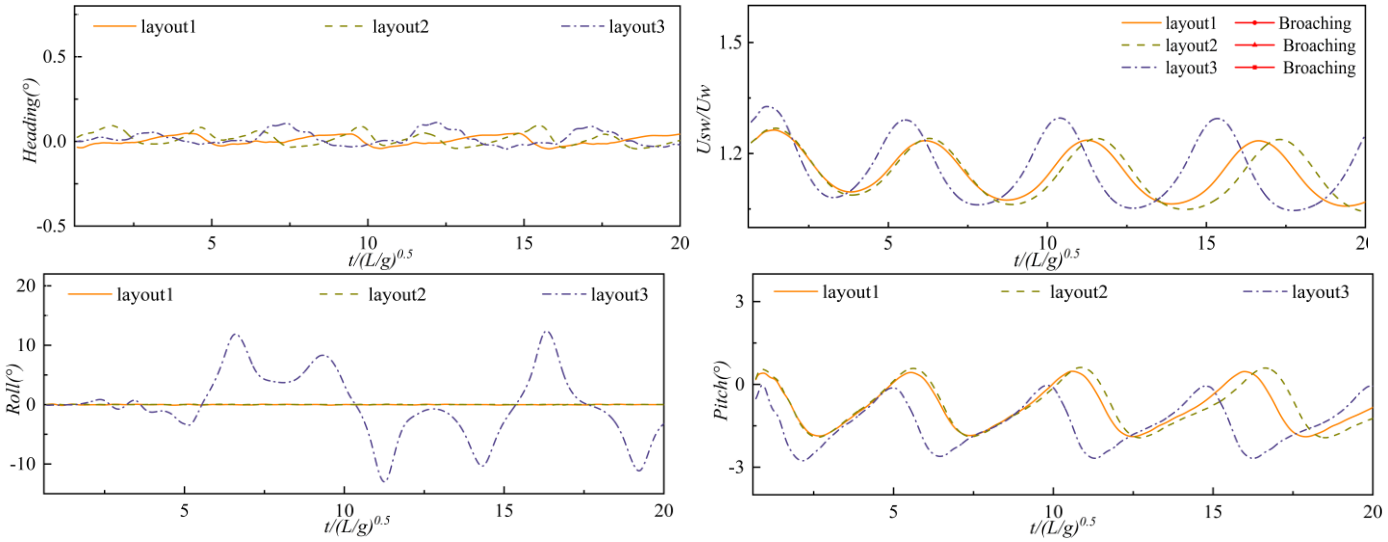
Table 5 The working condition with ak=0.140

λ/L	Fr	ak	β	Layout
0.5	0.45	0.140	0°	
0.7				
0.9				
1.1				Layout1
1.3				Layout2
1.5				Layout3
1.7				
1.9				
2.1				

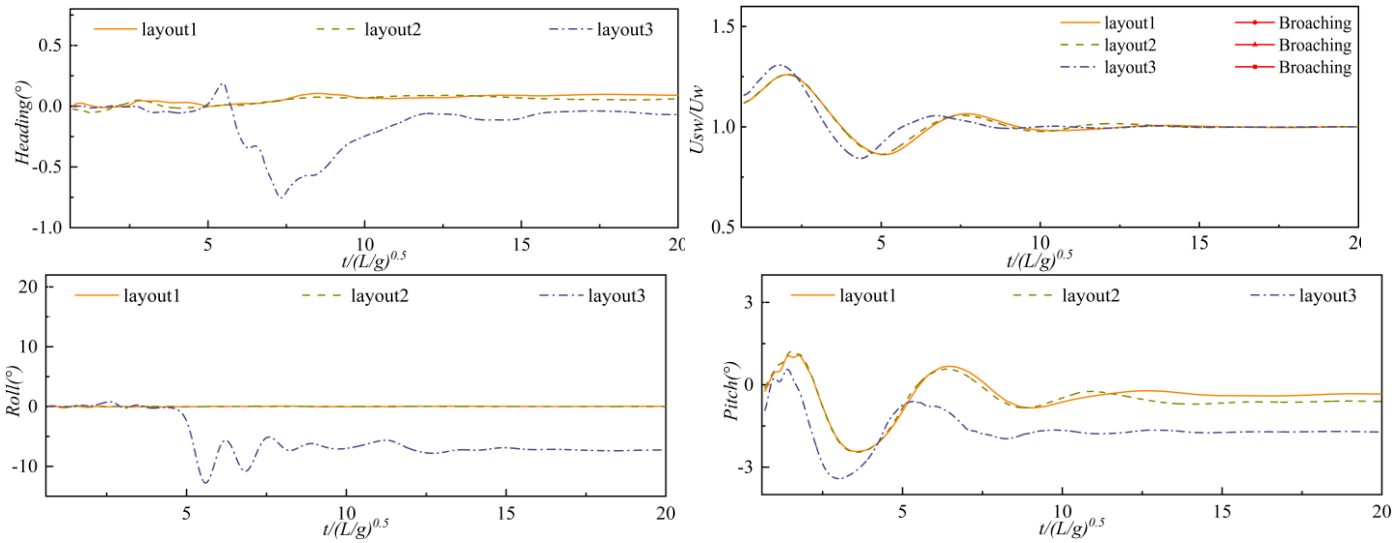
In this paper, specific criteria are established to ascertain the occurrence of surf-riding and broaching instability in the navigation of a trimaran. The projection of ship instantaneous speed to the wave direction is denoted as U_{sw}, while U_w represents the wave speed. When a ship is "captured" by waves, its navigational velocity aligns with the wave speed, ceasing to exhibit periodic variations. Marginal surf-riding is identified when $U_{sw} > 0.9U_w$ [27], surf-riding is identified when $U_{sw} = U_w$, when a ship's instantaneous speed is slightly higher than the wave speed and the wave crest is near the bow, the ship is blocked by the wave and forced to decelerate to the wave speed. This phenomenon is known as wave-blocking, which is less dangerous than surf-riding because it does not lead to capsizing, although once the wave-blocking phenomenon ceases, the ship may experience bow diving, and wave-blocking is identified when $U_{sw} > U_w$. [36, 37].

After a ship experiences the surf-riding phenomenon, it does not maintain a relatively constant navigational state. It may continue to steer through the waves or may suddenly turn sharply, resulting in a state where the ship fails to maintain straight-line navigation despite maximum steering force exertion, this is broaching phenomenon. The initial target heading here is 0°, with the nozzle deflection angle denoted as δ. The criteria for marginal broaching are identified when the bow yaw angle exceeds 20°(ξ_6>20°), the rudder

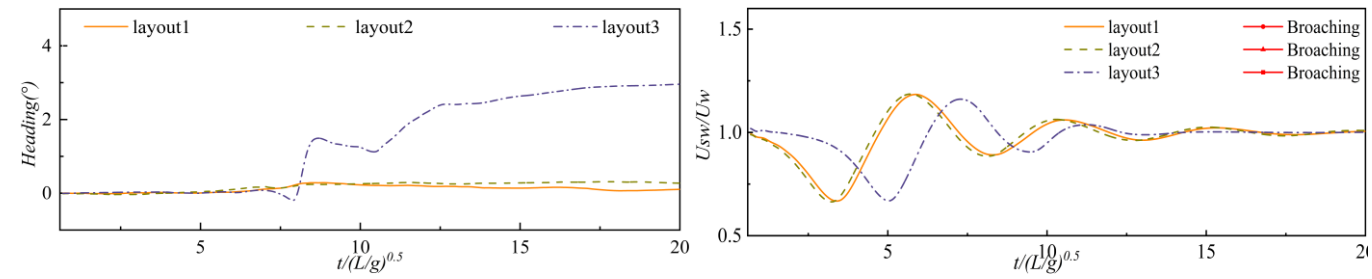
angle applied to maintain course during the turn reaches its maximum ($\delta=\delta_{max}$), and the bow yaw acceleration is greater than 0 ($\ddot{\xi}_6>0$), The criteria for broaching are $\xi_6>20°$, $\delta=\delta_{max}$, $\dot{\xi}_6>0$, $\ddot{\xi}_6>0$. where $\delta_{max}=35°$ and $\dot{\delta}=10°/s$ are used [27]. These criteria are used to mark the moments when the corresponding dangerous state occurs, with the purpose of analyzing the triggering mechanism and dynamic process of instability, rather than describing a continuous steady state. The criteria adopted in this study are based on instantaneous kinematic and control variables and are used to identify the moments when surf-riding, critical broaching, and broaching occur. However, this paper does not systematically vary or examine the effects of the initial wave phase, the initial position of the ship relative to the wave crest or trough, or small initial perturbations on the identification results of the criteria. Therefore, surf-riding or broaching events detected in a single deterministic simulation can only reflect the instability response under specific initial conditions and cannot be used to directly estimate the probability of instability occurrence under the corresponding wave conditions.

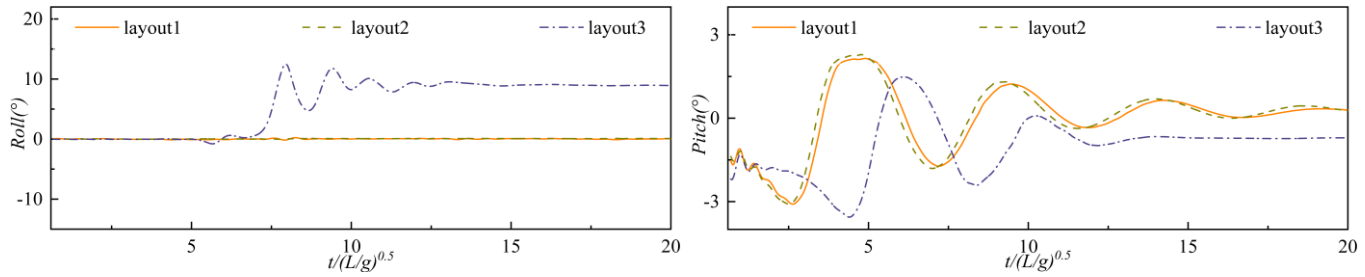


(a) heading, speed, roll and pitch motion (Fr=0.45, ak=0.096, β=0°, λ/L=0.9)

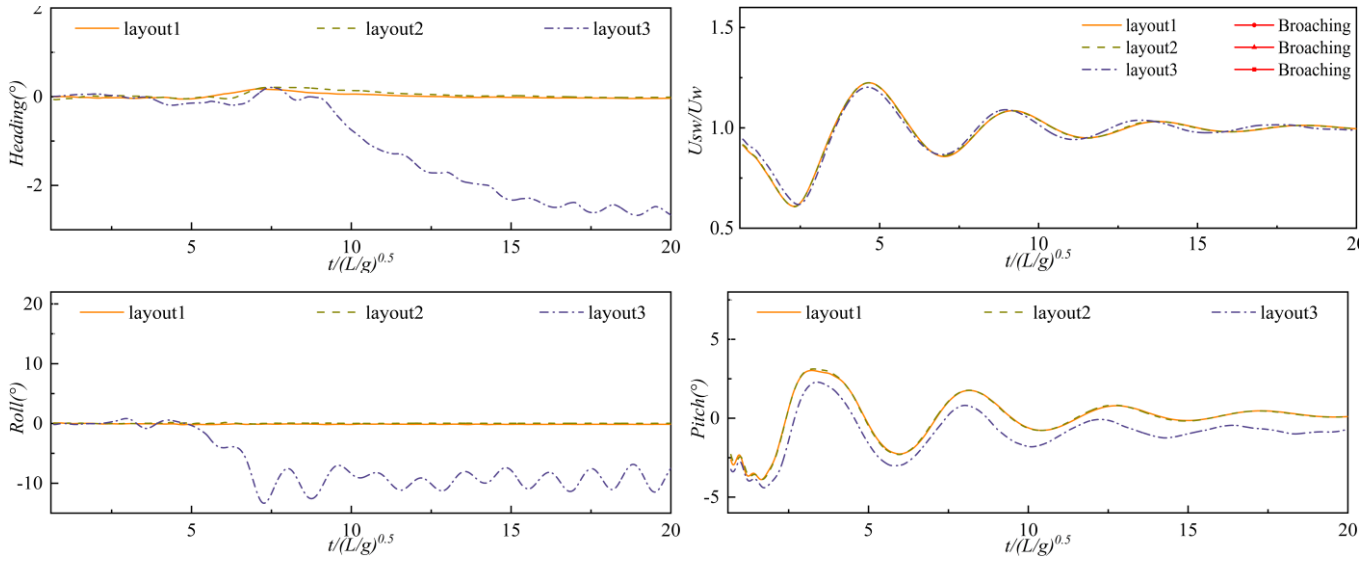


(b) heading, speed, roll and pitch motion (Fr=0.45, ak=0.096, β=0°, λ/L=1.1)

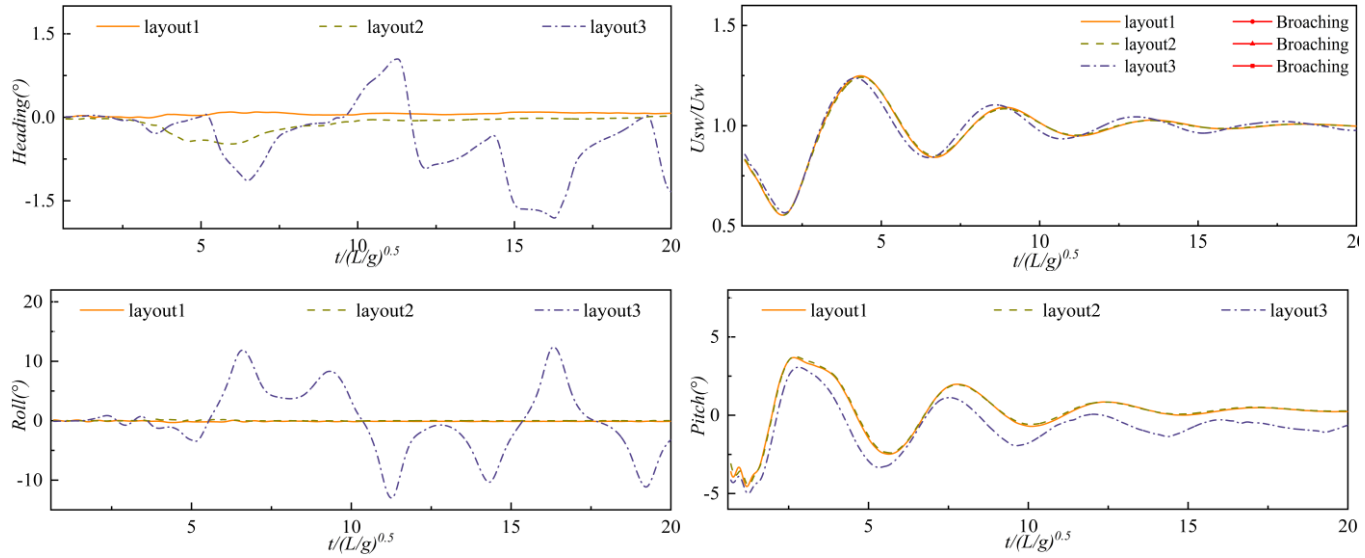




(c) heading, speed, roll and pitch motion (Fr=0.45, ak=0.096, β=0°, λ/L=1.3)



(d) heading, speed, roll and pitch motion (Fr=0.45, ak=0.096, β=0°, λ/L=1.5)



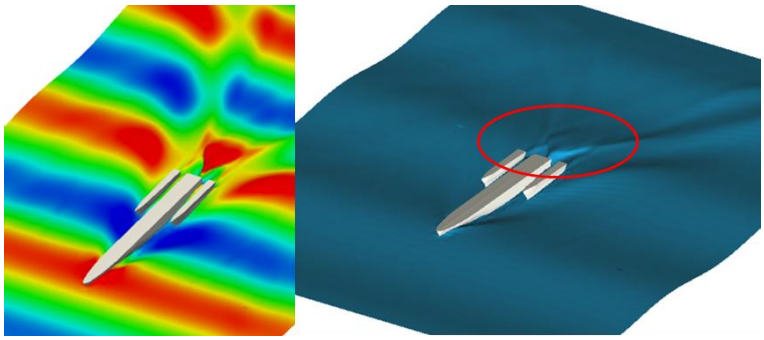
(e) heading, speed, roll and pitch motion (Fr=0.45, ak=0.096, β=0°, λ/L=1.7)

Fig. 6 The time history results at various wavelength without broaching occurrence

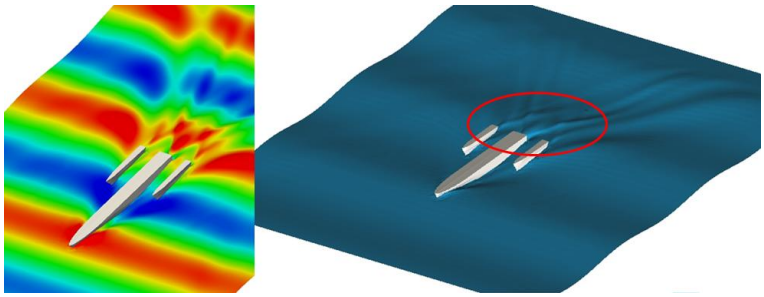
Figure 6 shows the time history of heading, speed, rolling, and pitching for a trimaran with different side-hull layouts at Fr=0.45. The orange solid lines represent Layout 1. The dark yellow dashed lines represent Layout 2. The dark blue dash-dot lines represent Layout3. As can be seen in Figure 6, broaching is indicated in red on the speed graph.

Figure 6 shows that under the following wave condition with wave steepness ak=0.096. The heading and rolling motions of Layouts 1 and 2 remain relatively stable, showing weak wave-ship coupling responses. In contrast, Layout 3 exhibits larger heading deviations and rolling amplitudes over the entire wavelength

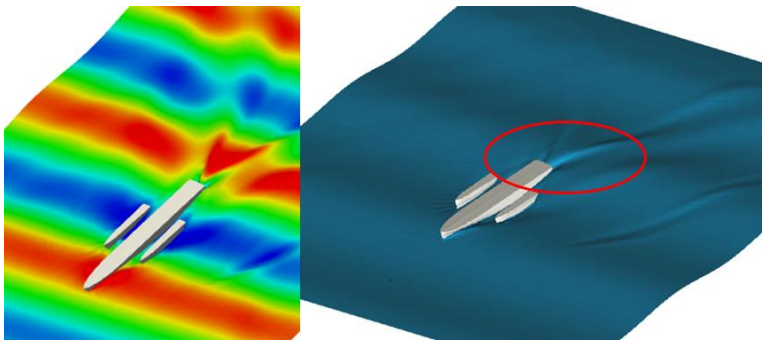
range, with significant nonlinear motion characteristics during the riding stage, and lower pitching amplitudes compared with the other two layouts. Owing to the forward shift of the side hulls in Layout 3, the uniformity of the flow field at the bow of the main hull is directly disturbed and disrupted, leading to flow separation and uneven pressure distribution at the bow, which further amplifies the heading deviation. Specifically, when the side hulls are continuously impacted by wave crests on one side, the local immersion depth increases and wave loads rise significantly, while the side hulls on the opposite side emerge and experience a sharp reduction in forces. Such asymmetric wave loads directly lead to the continuous amplification of rolling motions, resulting in high rolling amplitudes over the entire wavelength range. The layout with aft-positioned side hulls maintains the original pattern of the bow flow field of the main hull, avoiding concentrated wave excitation at the bow. Meanwhile, the aft-positioned side hulls provide strong constraint on the stern flow field of the main hull, thus improving the heading-keeping ability. Among them, Layout 2 weakens the wave-making interference between the side hulls and the main hull and reduces the oscillatory responses. The forward-positioned side hulls directly interfere with the incoming flow at the bow of the main hull and break the uniformity of the flow field, resulting in significantly increased wave excitation on the side hulls. Under the condition of ak=0.096, the layout with aft-positioned side hulls is the optimal layout to suppress motion instability during the following-wave stage. Therefore, for the purpose of motion stability during the following-wave stage, the layout form of aft-positioned side hulls plus properly increased transverse spacing should be preferentially adopted.



(a) The wave elevation of Layout 1 (Fr=0.45, H=100, ak=0.096, β=0°, λ/L=1.1)



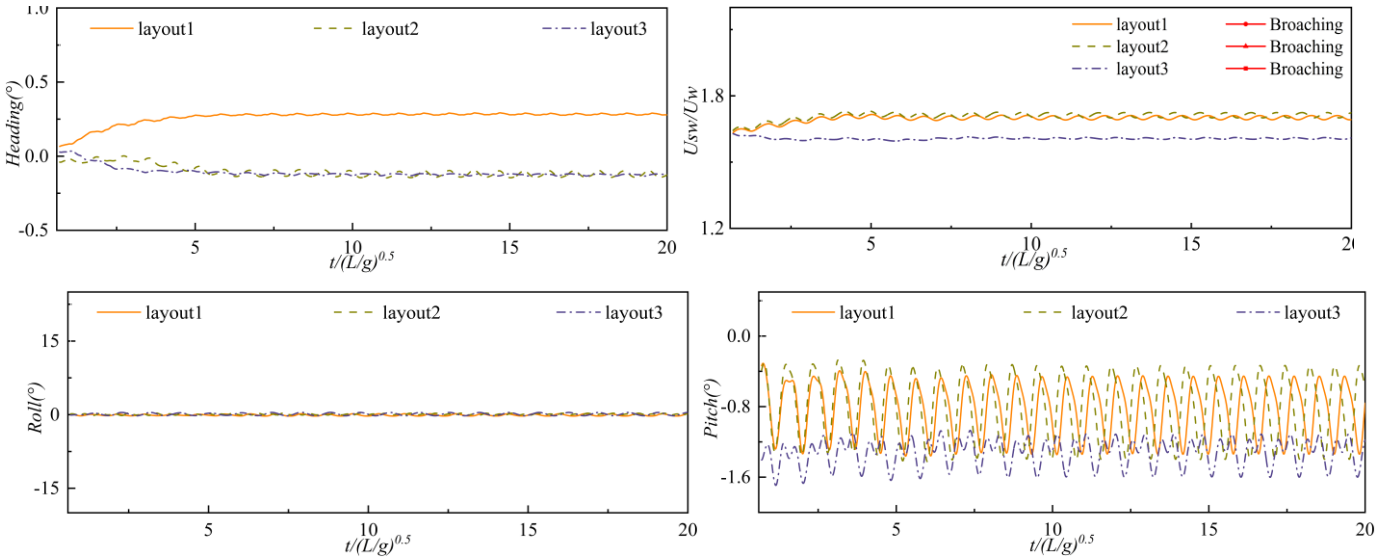
(b) The wave elevation of Layout 2 (Fr=0.45, H=100, ak=0.096, β=0°, λ/L=1.1)



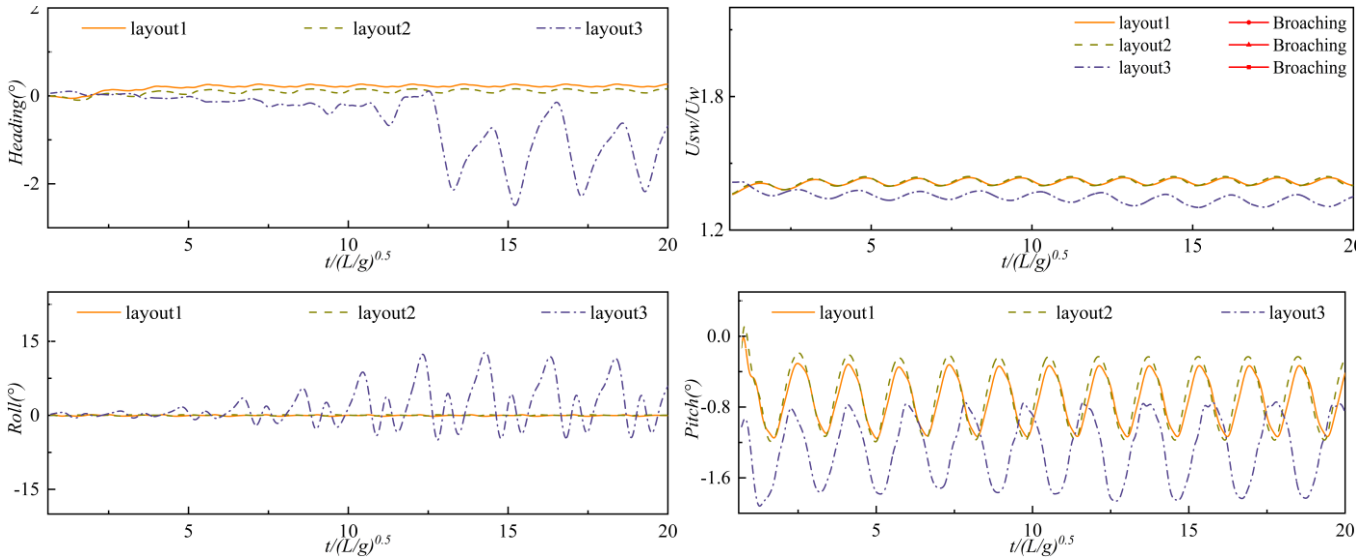
(c) The wave elevation of Layout 3 (Fr=0.45, H=100,ak=0.096, β=0°, λ/L=1.1)

Fig. 7 The wave elevation of different layouts without broaching

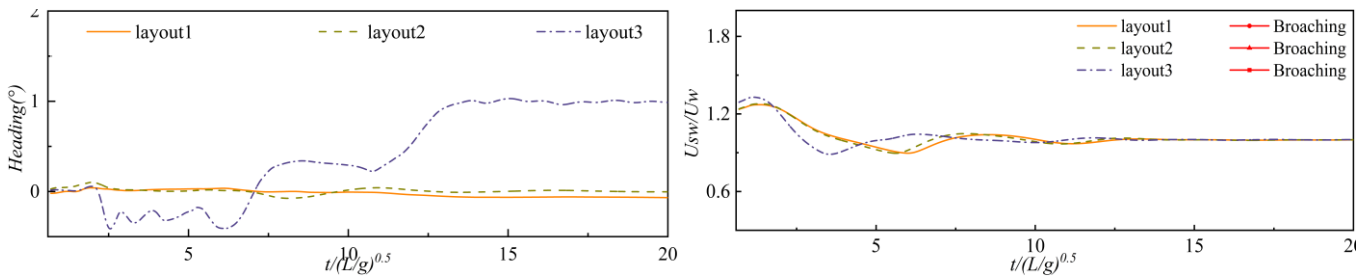
Figure 7 presents the wave elevation for a trimaran with different side hull layouts in λ/L=1.1. Figures 7(a)(b)(c) represent Layout 1, 2, and 3 respectively. From Figure 7(a), Layout 1 cause less water flow interference, leading to better vessel motion stability. The increased side-hull spacing in Layout 2 results in more water diffusion and energy dissipation at the stern. This may alter the pitching motion compared to Layout 1, see Figure 6(b), yet it still maintains good motion stability. Layout 3 directly disrupts the forward water flow, creating greater interference. Consequently, the ship motion response becomes more complex and unstable. Under this condition, the trimaran exhibits larger rolling and pitching amplitudes, more irregular motion, rapid speed changes, and some heading control fluctuations, consistent with Figure 6(b).

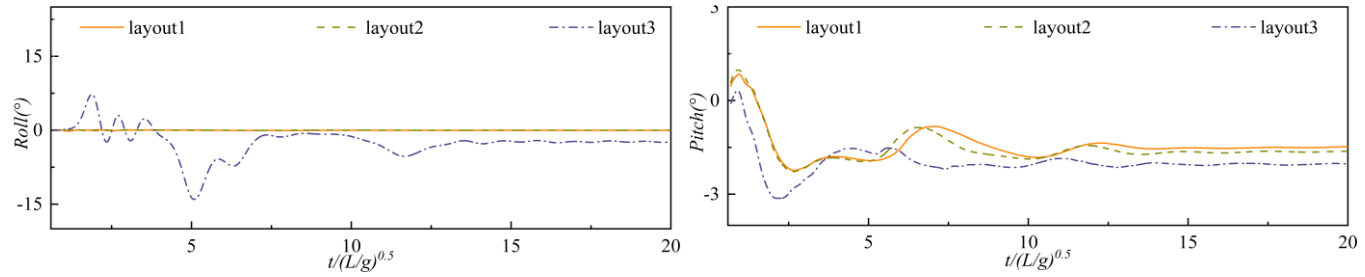


(a) heading, speed, roll and pitch motion (Fr=0.45, ak=0.140, β=0°, λ/L=0.5)

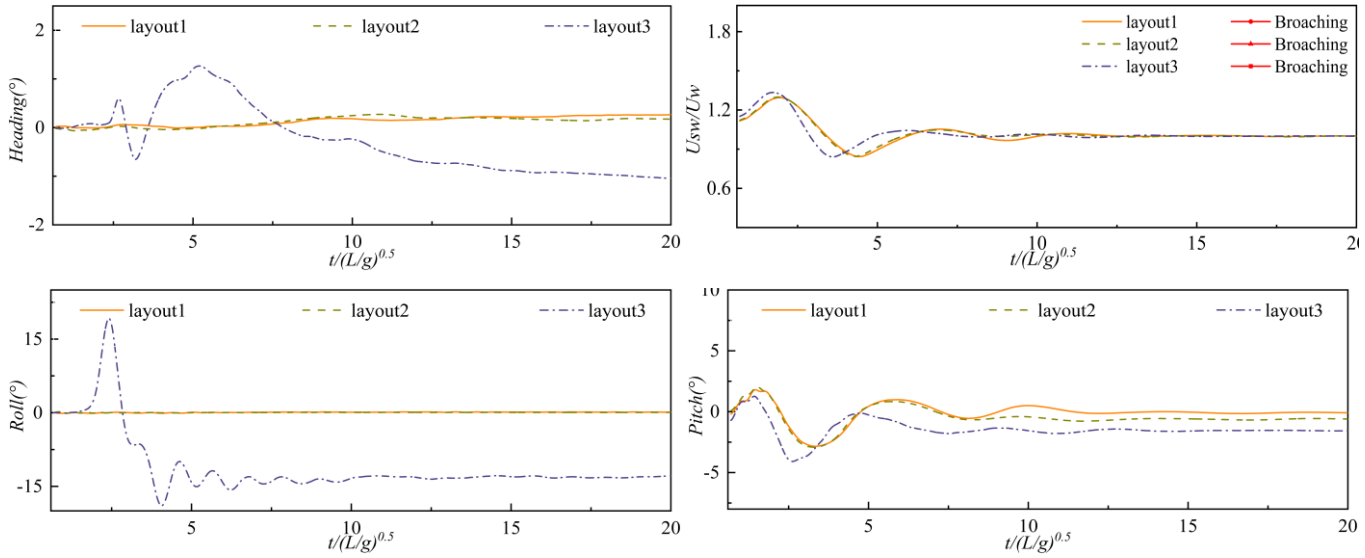


(b) heading, speed, roll and pitch motion (Fr=0.45, ak=0.140, β=0°, λ/L=0.7)

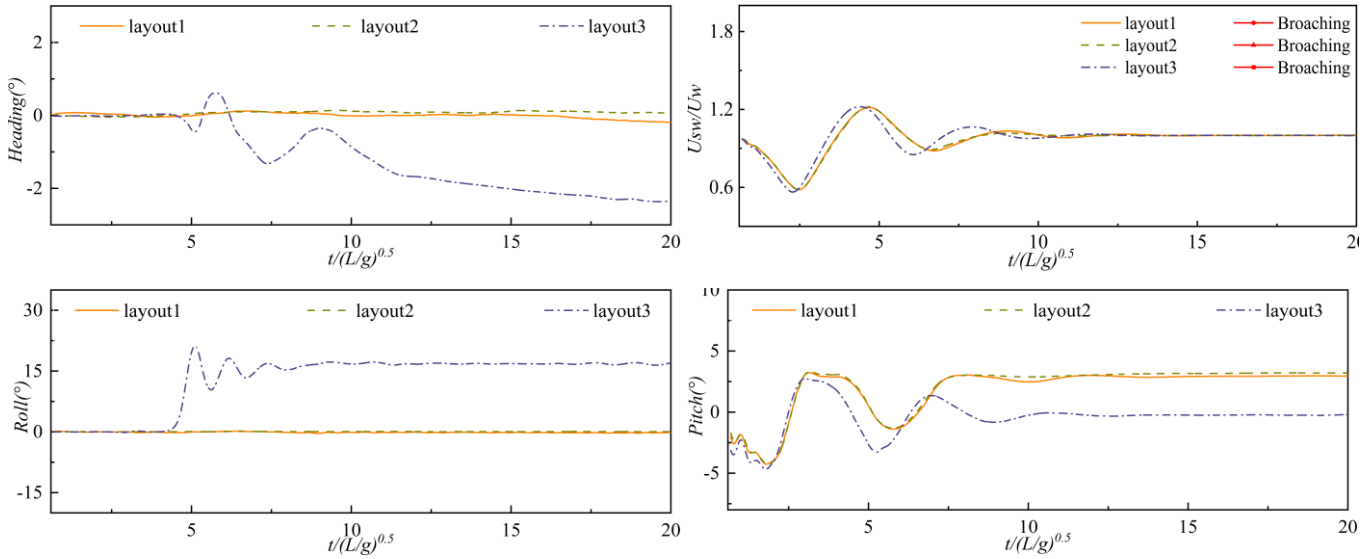




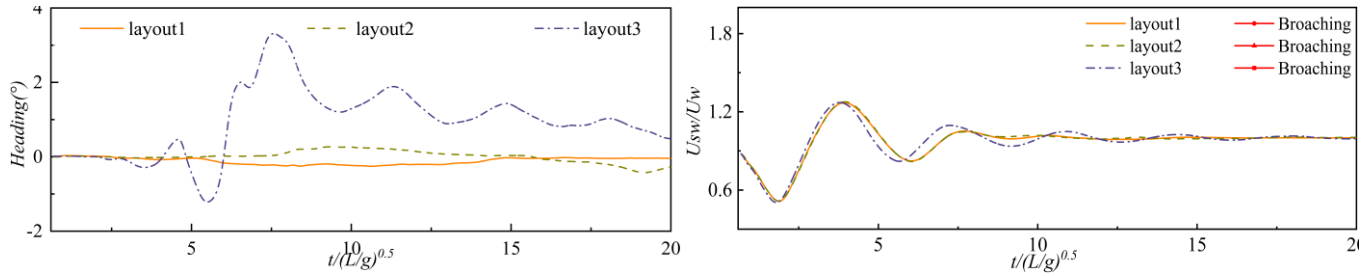
(c) heading, speed, roll and pitch motion (Fr=0.45, ak=0.140, β=0°, λ/L=0.9)

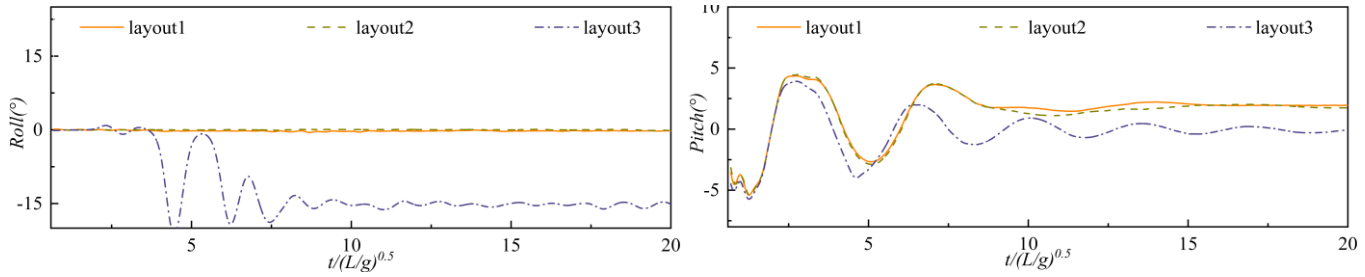


(d) heading, speed, roll and pitch motion (Fr=0.45, ak=0.140, β=0°, λ/L=1.1)

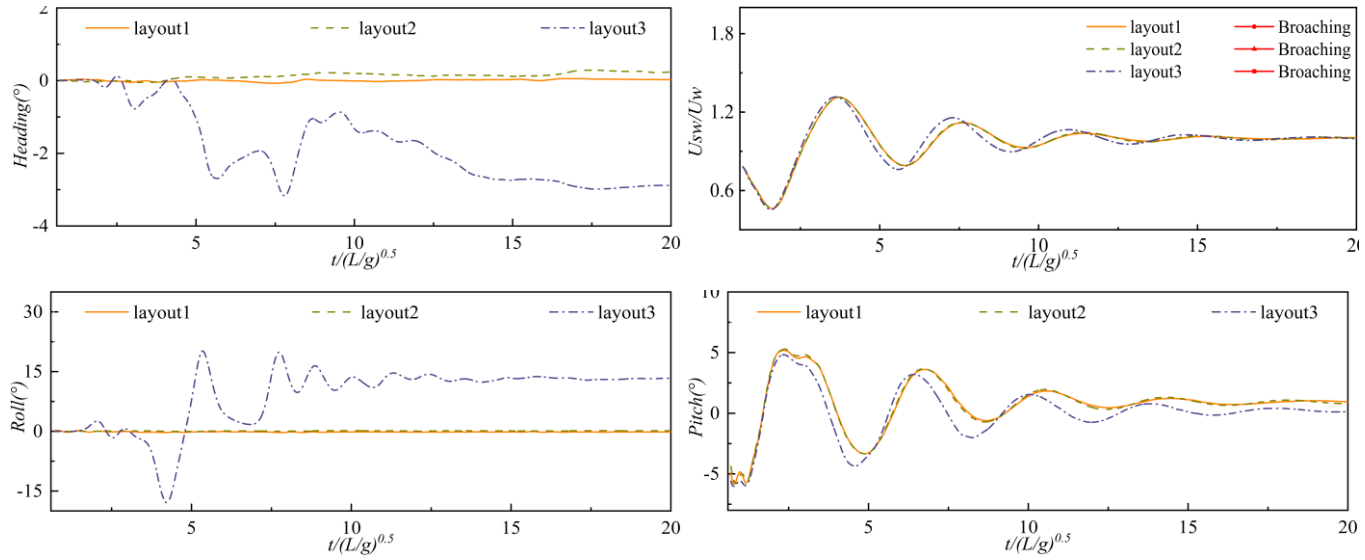


(e) heading, speed, roll and pitch motion (Fr=0.45, ak=0.140, β=0°, λ/L=1.3)

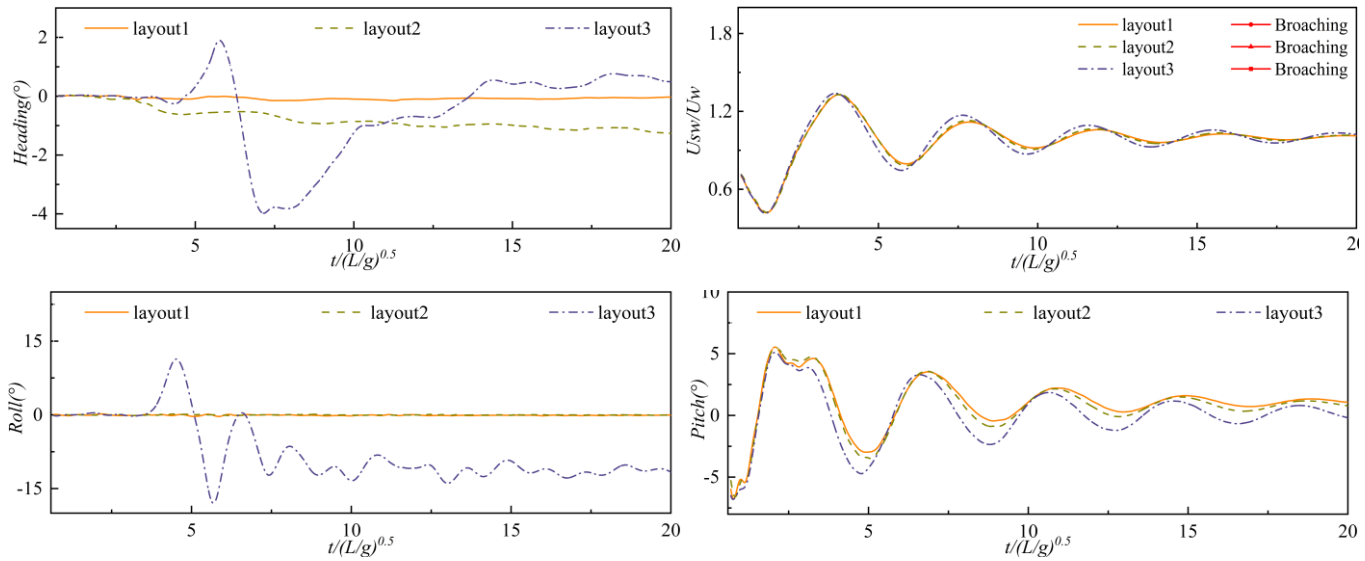




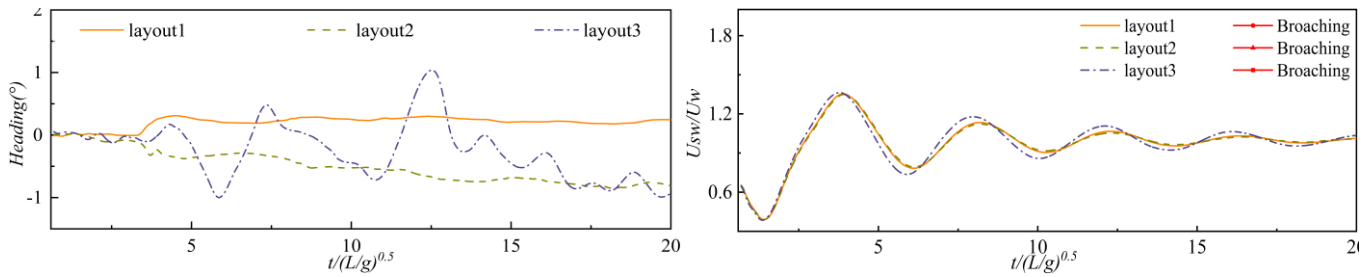
(f) heading, speed, roll and pitch motion (Fr=0.45, ak=0.140, β=0°, λ/L=1.5)

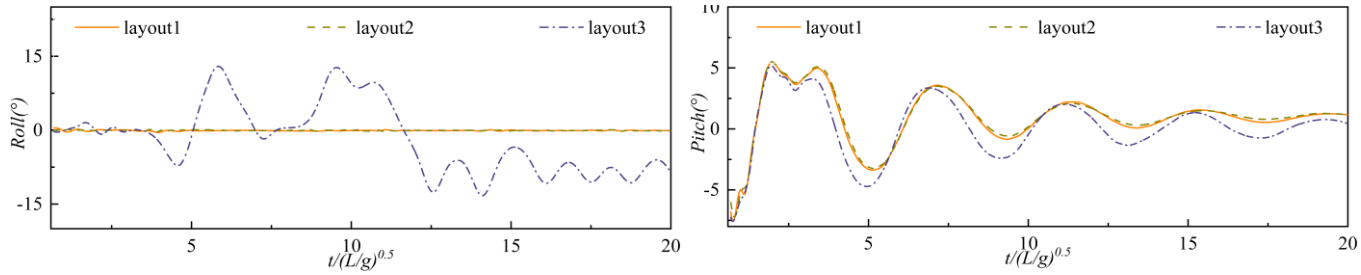


(g) heading, speed, roll and pitch motion (Fr=0.45, ak=0.140, β=0°, λ/L=1.7)



(h) heading, speed, roll and pitch motion (Fr=0.45, ak=0.140, β=0°, λ/L=1.9)



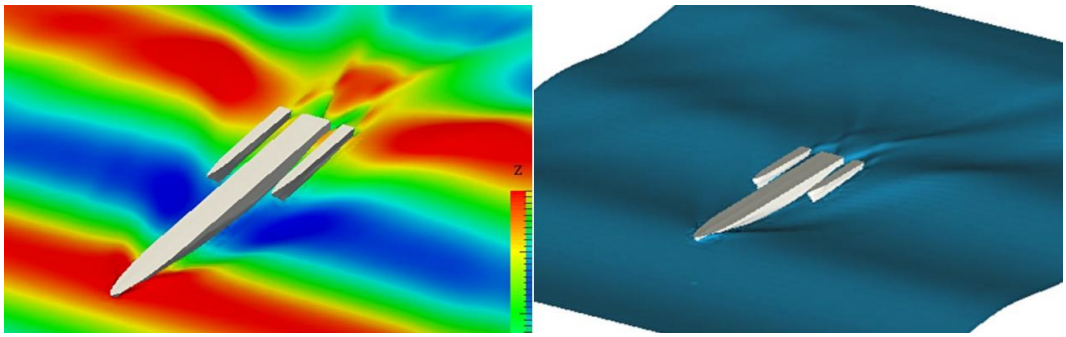


(i) heading, speed, roll and pitch motion (Fr=0.45, ak=0.140, β=0°, λ/L=2.1)

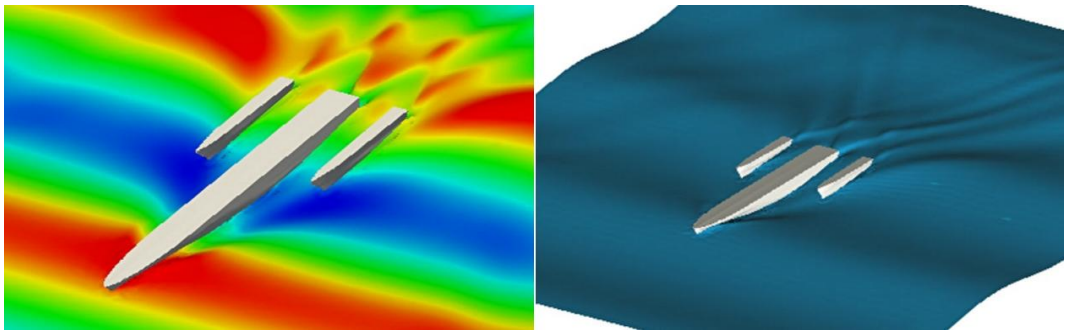
Fig. 8 The time history of computed results at various wavelength without broaching

Figure 8 presents the time histories of heading, speed, roll and pitch for the three layouts under the conditions of Fr=0.45, ak=0.140 and β=0°. As observed from Figure 8, Overall, Layouts 1 and 2 exhibit similar heading stability. Although Layout 3 shows slight deviations, most variations are within 4 degrees, indicating that the trimaran possesses good course-keeping stability under the three different layouts. The ship speed varies with wavelength. At $\lambda/L \geqslant 0.9$, nonlinear effects including wave interactions around side hulls and intermittent emergence of side hulls lead to short-term oscillations in speed and pitch, which are mainly caused by the nonlinear effects of waves on hull motions [38]. In particular, when $\lambda/L > 0.8$, the influence of wave nonlinearity increases sharply, and significant periodic disturbances appear when $ak > 0.1$. In addition, the critical wavelength ratio $\lambda/L \approx 0.9$ is close to the roll-heave coupled resonance zone of the trimaran [39]. At this point, the relative motion phase between the hull and waves amplifies initial disturbances, making the ship prone to transient motion instability in following waves, characterized by short-term oscillations in speed and pitch. Furthermore, under long wavelengths, the wake vortex shedding induced by hull motions takes longer to reach a steady state, resulting in oscillations of hydrodynamic loads at the initial stage [39]. Comparison between Layouts 1 and 2 shows that increasing the transverse separation can further weaken the wave-making interference and wave diffraction effects between the main hull and side hulls and allow more sufficient diffusion of wave energy at the stern. Thus, the transverse wave impact on the hull under high wave steepness is effectively reduced, so the roll and speed fluctuations of Layout 2 are slightly smaller than those of Layout 1. Under high wave steepness, Layout 3 shows stronger disturbance to the bow flow field due to the relatively forward side hulls, resulting in more significant heading fluctuations and weaker overall motion stability than Layouts 1 and 2. Under the condition of ak = 0.140, the stability of Layouts 1 and 2 is better than that of Layout 3. If the ship is required to sail in following seas with high wave steepness, the stern-arranged side-hull layout is strongly recommended.

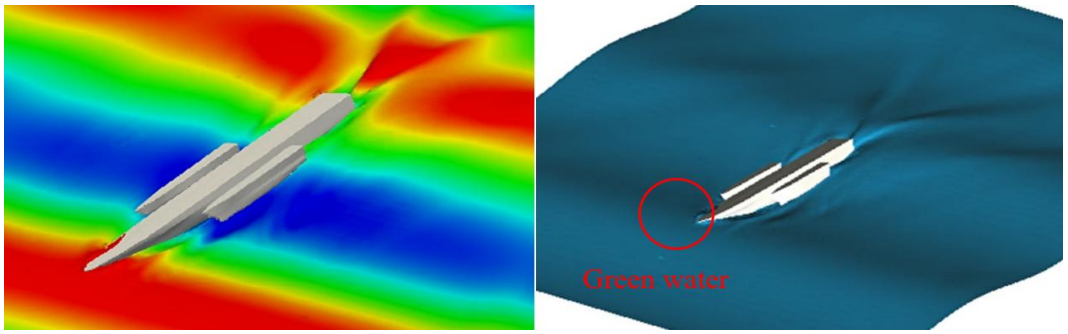
As shown in Figures 9(a)(c), the bow and stern are positioned at two adjacent wave crests. In Layout 1, the side hulls are located near the stern wave crest, while in Layout 3, the side hulls are positioned within the wave trough. This results in distinct phase relationships. When the side hulls are situated in the trough, the local flow field around the side hulls is inevitably affected. During rolling, the side hull in the trough undergoes drastic changes in submersion depth, leading to highly asymmetric restoring forces/moments over the roll cycle. The altered flow field generates substantial asymmetric hydrodynamic forces, thereby causing significant roll oscillations and a steady offset.



(a) The wave elevation of Layout 1 (Fr=0.45, ak=0.140, β=0°, λ/L=1.1)



(b) The wave elevation of Layout 2 (Fr=0.45, ak=0.140, β=0°, λ/L=1.1)



(c) The wave elevation of Layout 3 (Fr=0.45, ak=0.140, β=0°, λ/L=1.1)

Fig. 9 The wave elevation of different layouts without broaching.

Figure 9 shows that Layout 1 offers the best motion stability with steady responses. Layout 2 despite increased stern wave diffusion and energy loss, still maintains good stability and shows adaptability. Layout 3 due to greater water flow interference from its side-hull position, has complex and unstable motion responses. It has larger rolling amplitudes, rapid speed changes, and heading control fluctuations. During surf-riding, the bow is almost fully submerged, the phenomenon of green water occurred, leading to larger hull motion responses. The uneven forces on the hull, caused by complex water flow interference, further worsen the motion instability.

4.2 The impact of layout on broaching

In this section, the main focus is on studying the impact of different side-hull layouts on the broaching of a trimaran in quartering stern waves. Initially, the influence of the ship's initial speed on the broaching characteristics of the trimaran is studied. A comparative analysis of the effects of three side-hull layouts on the motion characteristics of the trimaran under low, medium, and high-speed conditions is conducted, with detailed conditions referred to in Table 6. Subsequently, the performance of the three layouts under different wavelength conditions in steep waves is explored and compared, with detailed conditions presented in Table 7.

Table 6 The working condition of various Fr

Fr	λ/L	ak	β	*Layout*
0.35	1.1	0.096	30°	*Layout*1 *Layout*2 *Layout*3
0.38				
0.40				
0.45				
0.50				
0.55				
0.60				
0.65				

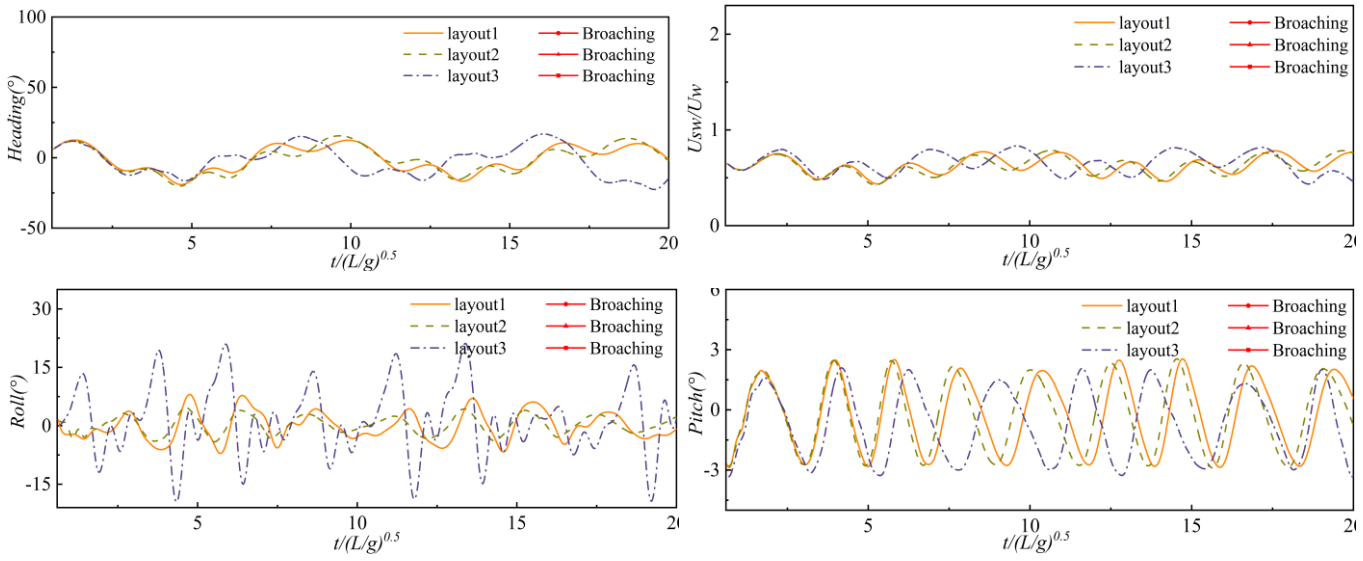
Table 7 The working condition of various λ/L

λ/L	Fr	ak	β	*Layout*
0.9	0.45	0.140	30°	*Layout*1 *Layout*2 *Layout*3
1.1				
1.3				
1.5				
1.7				

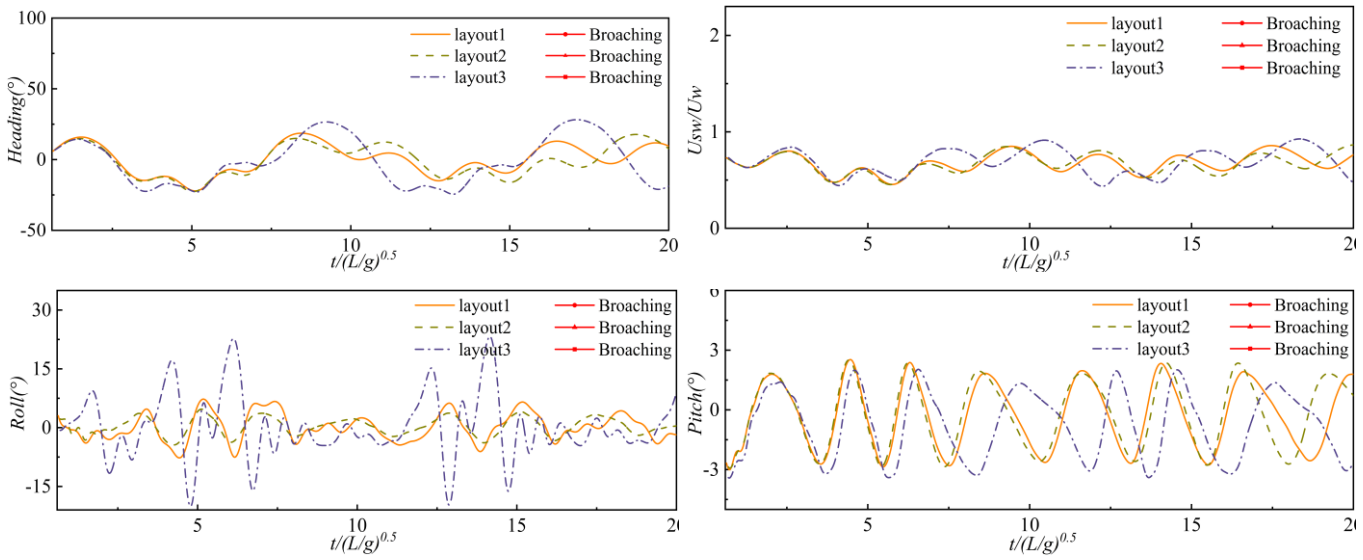
Table 8 The occurrence of broaching in different layouts

Fr	0.35	0.38	0.40	0.45	0.50	0.55	0.60	0.65
	O_{MB}/O_B	O_{MB}/O_B	O_{MB}/O_B	O_{MB}/O_B	O_{MB}/O_B	O_{MB}/O_B	O_{MB}/O_B	O_{MB}/O_B
*Layout*1	×	×	×	√	×	×	×	×
*Layout*2	×	×	×	√	×	×	√	×
Layout3	×	×	×	√	√	√	×	×

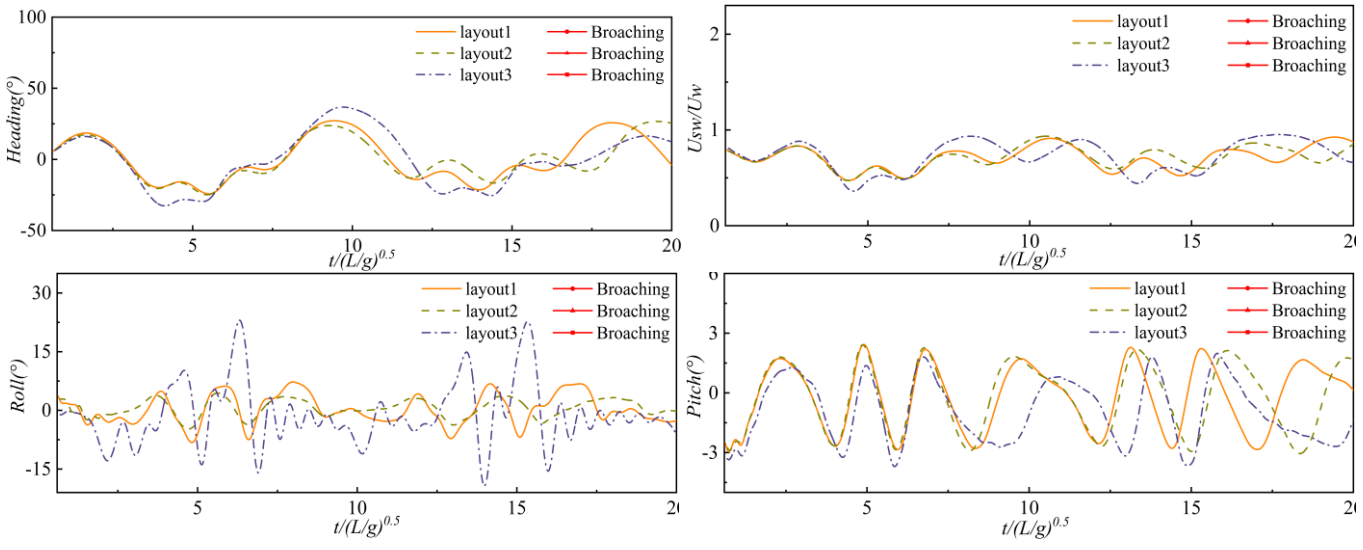
The computational results in Table 8 illustrate the occurrence of broaching for the trimaran sailing in quartering stern waves at various side-hull layouts and initial forward speeds. In the table, O_{MB} represents marginal broaching, and O_B represents broaching. It can be observed that at a speed of Fr= 0.35, the relative motion between the ship and the waves is slower, and the likelihood of wave capture is lower, with all three layouts exhibiting a more stable navigational state. When the speed Fr increases to 0.45, broaching occurs in all three configurations. It can be observed that with the increase in speed, broaching is more easily triggered in different layouts, and Layout 3 is more sensitive to the increase in speed. The analysis of the effect of initial velocity in this study is limited to one wave steepness, one wavelength ratio, and one wave direction angle. Therefore, the unstable responses identified under these discrete velocity conditions cannot be used to determine general critical velocities for surf-riding or broaching that are applicable to other wave conditions. The unstable responses under different configurations also did not exhibit a consistent monotonic variation with initial velocity, suggesting that the effect of initial velocity may be related to the relative encounter state between the ship and the waves. Further systematic calculations under different wave parameters are needed, together with repeated simulations under the same nominal conditions but with variations in the ship's initial position, the initial wave phase, or the initial motion perturbation, to examine the robustness of the identified instability range and assess the probability of instability occurrence.



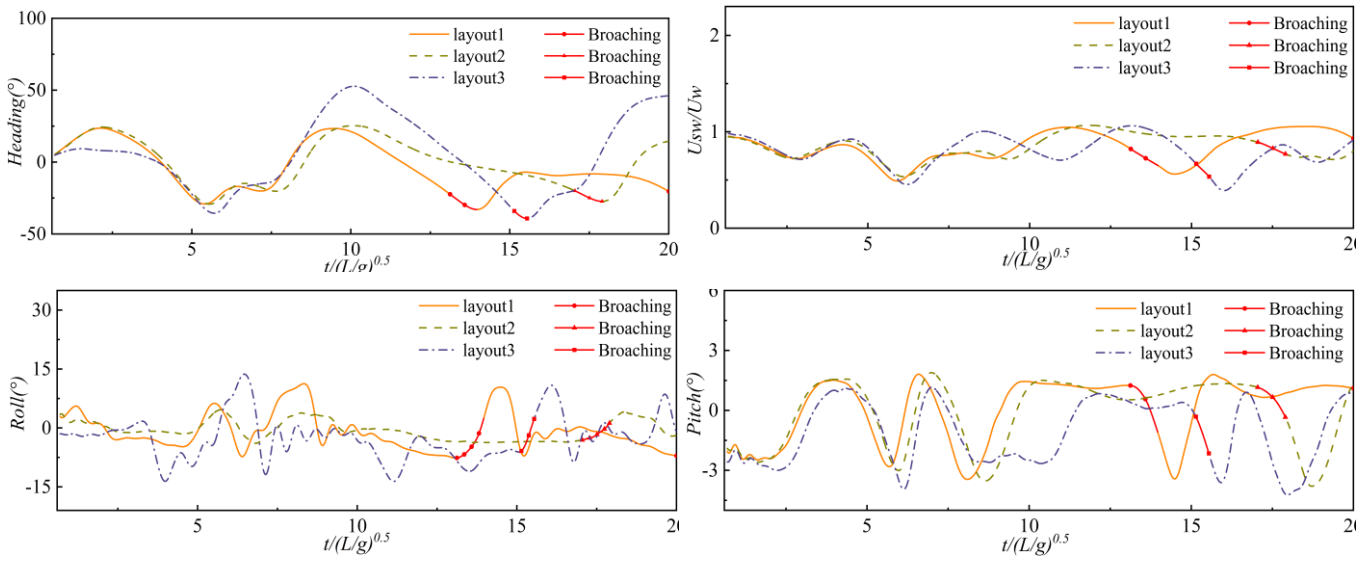
(a) heading, speed, roll and pitch motion (Fr=0.35, ak=0.096, β=30°, λ/L=1.1)



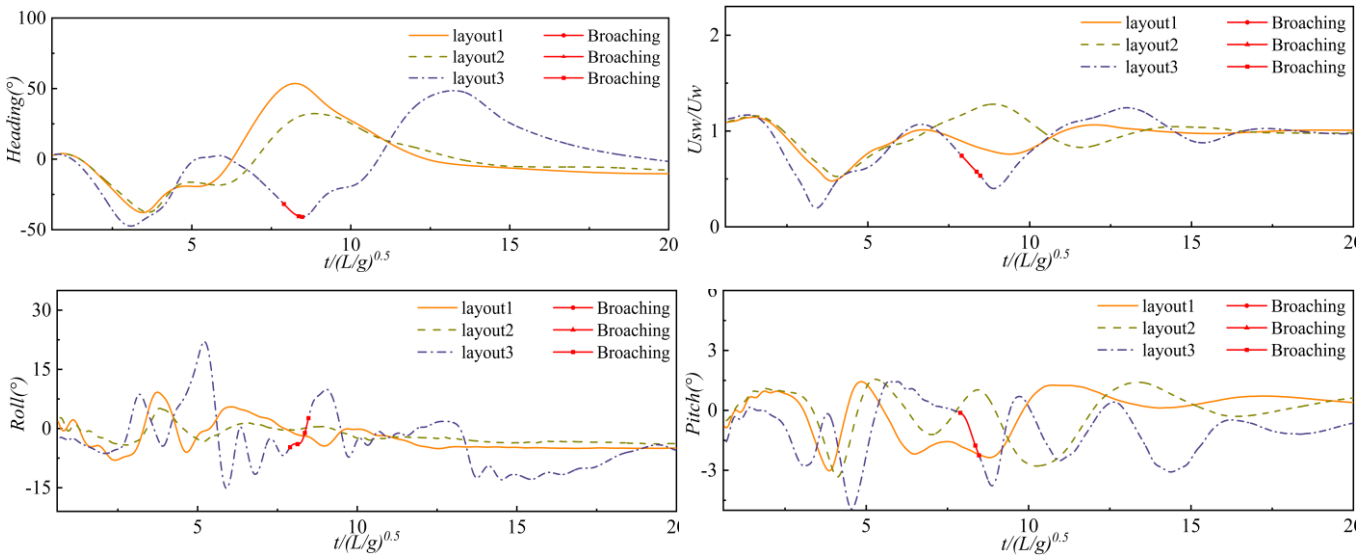
(b) heading, speed, roll and pitch motion (Fr=0.38, ak=0.096, β=30°, λ/L=1.1)



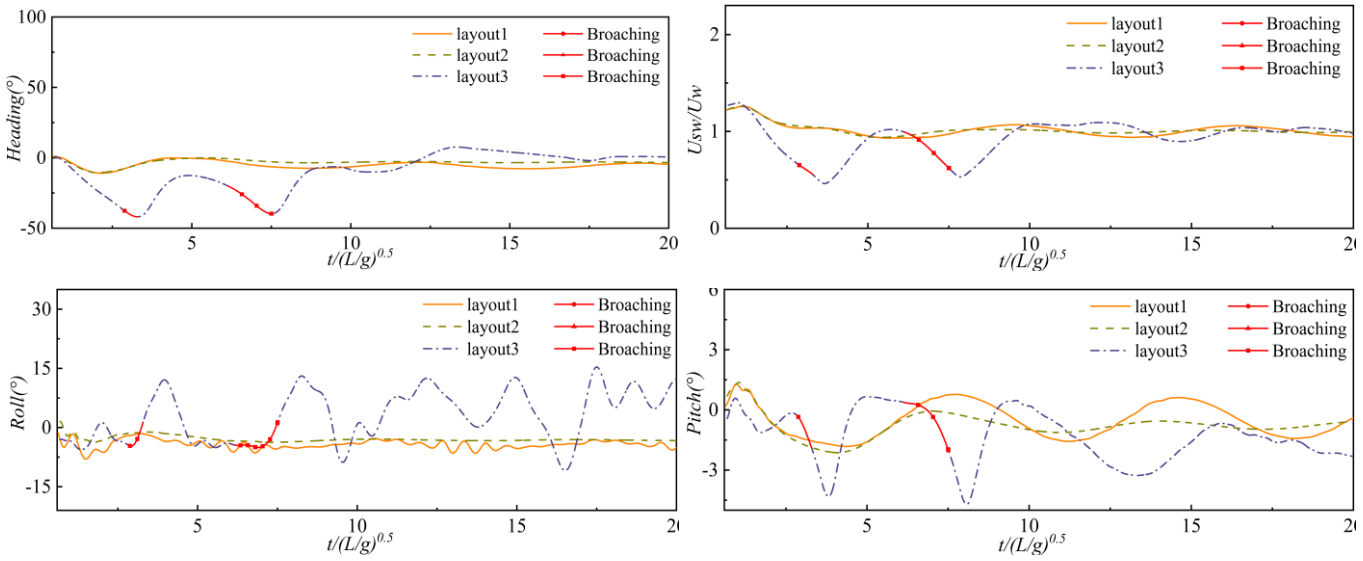
(c) heading, speed, roll and pitch motion (Fr=0.40, ak=0.096, β=30°, λ/L=1.1)



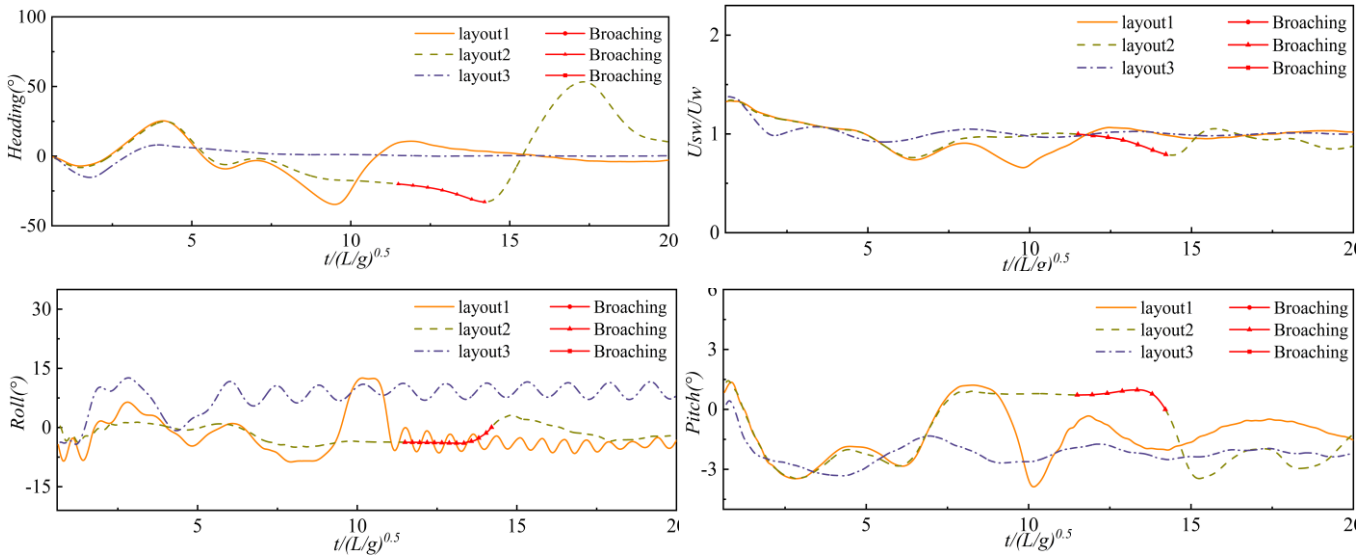
(d) heading, speed, roll and pitch motion (Fr=0.45, ak=0.096, β=30°, λ/L=1.1)



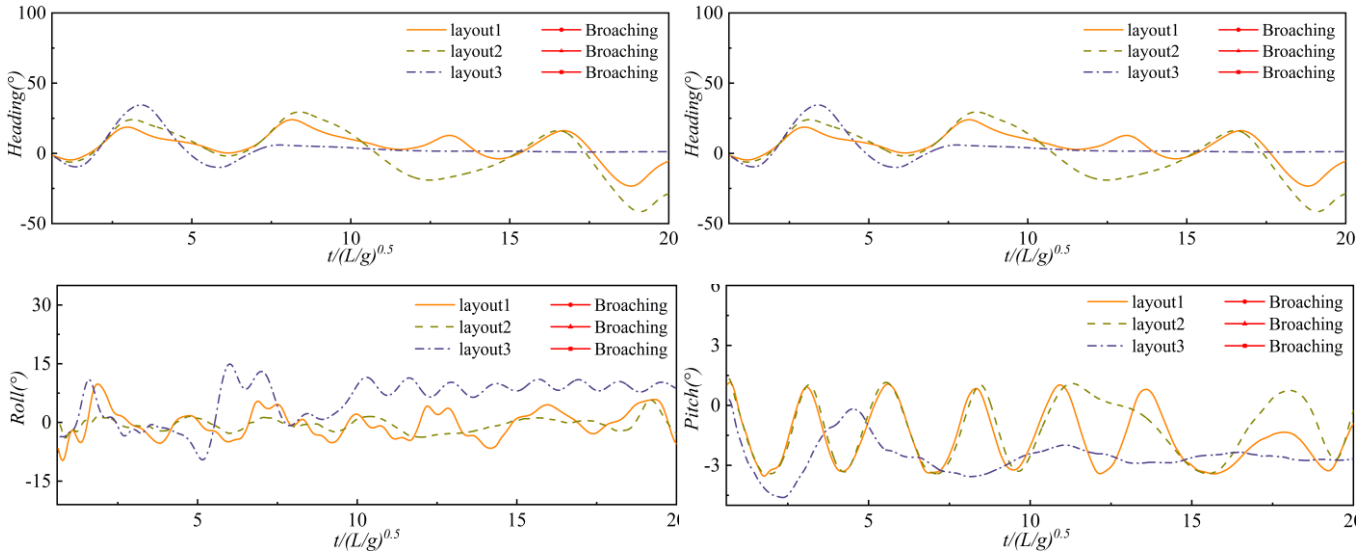
(e) heading, speed, roll and pitch motion (Fr=0.50, ak=0.096, β=30°, λ/L=1.1)



(f) heading, speed, roll and pitch motion (Fr=0.55, ak=0.096, β=30°, λ/L=1.1)



(g) heading, speed, roll and pitch motion (Fr=0.60, ak=0.096, β=30°, λ/L=1.1)

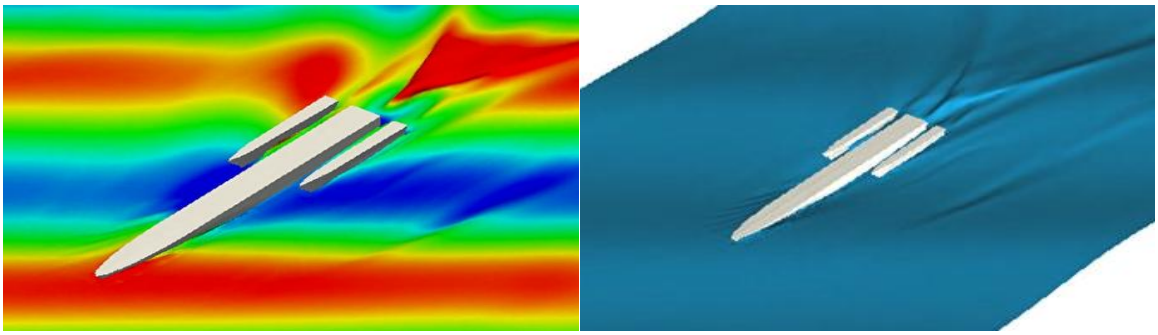


(h) heading, speed, roll and pitch motion (Fr=0.65, ak=0.096, β=30°, λ/L=1.1)

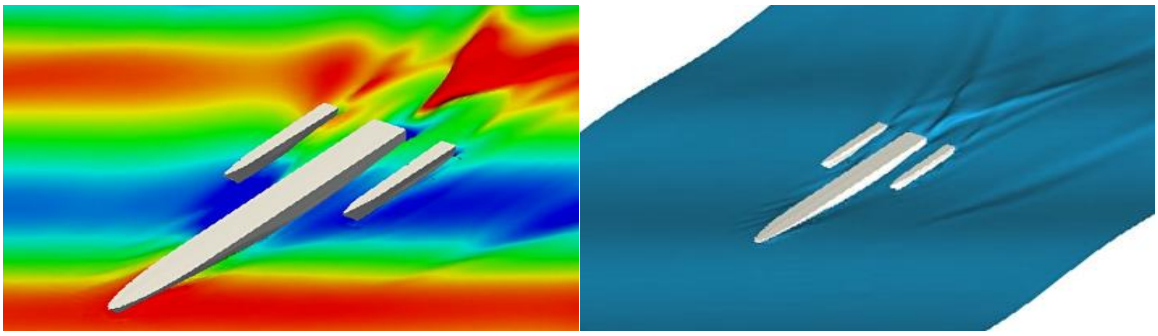
Fig. 10 The time history of computed results at various Fn with broaching

Figure 10 presents the time history of heading, rudder, speed, rolling, and pitching for the three side-hull configurations under the conditions of ak=0.096, β=30°, λ/L=1.1, and Fr=0.35~0.65. From the heading graphs in Figure 10, it can be observed that the heading deviation fluctuations for the three layouts follow a certain pattern. Relatively speaking, Layout 3 exhibits larger amplitude fluctuations, with deviations close to 50° under all speeds except Fr=0.35 and 0.60. Overall, during the Fr range of 0.35~0.45, all three layouts show fluctuations, with Layout 3 being more pronounced. Between Fr=0.55 and 0.65, the fluctuations are minor and quickly stabilize near 0°. Examining the speed graphs in Figure 10. It is found that both Layout 1 and Layout 2 undergo broaching at Fr = 0.45. Compared to Layouts 1 and 2, Layout 3 is more sensitive to changes in speed, Layout 3 exhibits broaching conditions at Fr = 0.45~0.55. After Fr=0.50, there are initial fluctuations in speed, which then tend to stabilize, with minimal broaching occurring. The forward shift of the outriggers in Layout 3 significantly affects its speed stability at different Fr levels. As Fr increases, the dynamic response of Layout 3 improves, reducing the occurrence of broaching. From the rolling graphs in Figure 10, it can be deduced that Layouts 1 and 2 exhibit relatively smaller amplitudes, yet they remain generally within the range of -15° to 15° , demonstrating satisfactory stability. Compared to Layout 1, Layout 2, which likely has an increased lateral spacing between the side hulls, shows a significant reduction in the rolling response amplitude. In contrast to Layout 1, Layout 3 maintains the same lateral spacing but increases

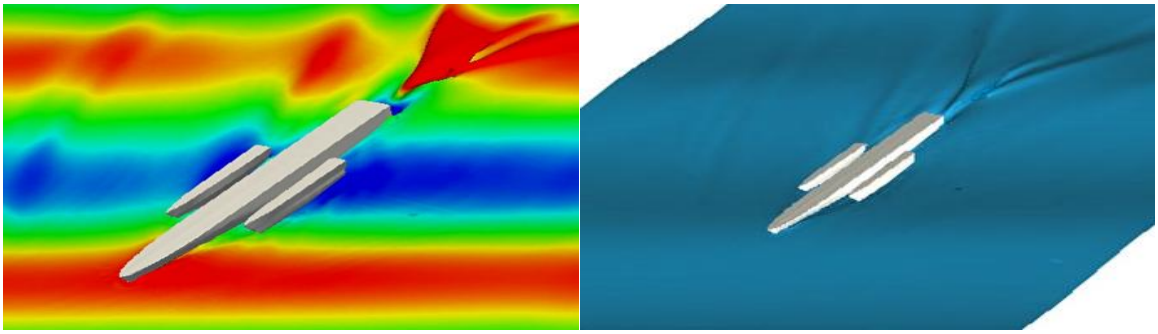
the longitudinal spacing, and as a result, experiences an increase in the rolling response amplitude. Regarding the pitching graphs in Figure 10, the pitching response amplitudes for all three layouts do not show significant deviations, oscillating within the range of -5° to 5°. After Fr=0.45, Layout 3 tends to stabilize in the later stages. With the exception of Fr=0.65, after Fr=0.50, Layouts 1 and 2 also approach stability.



(a) The wave height contour plot of Layout 1

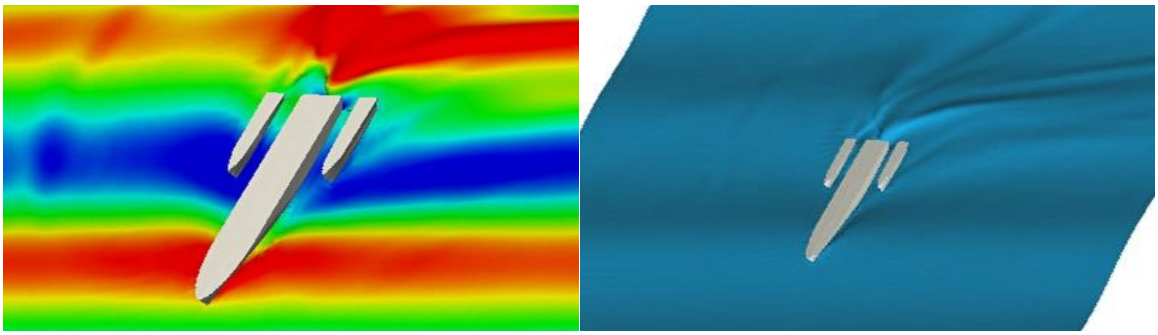


(b) The wave height contour plot of Layout 2

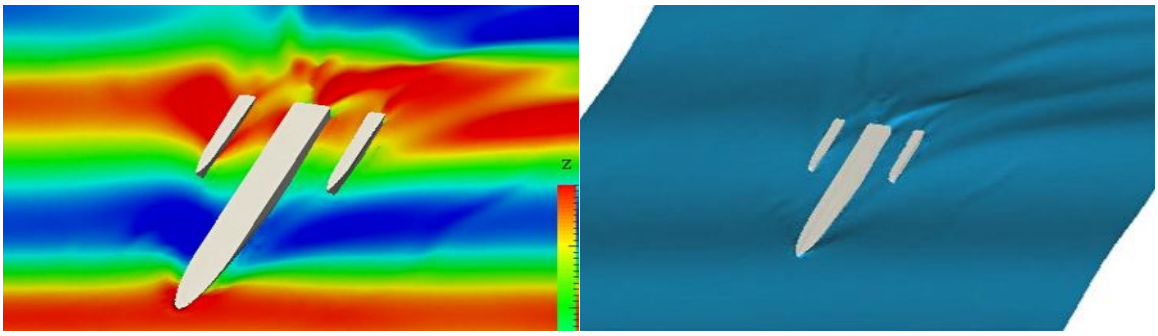


(c) The wave height contour plot of Layout 3

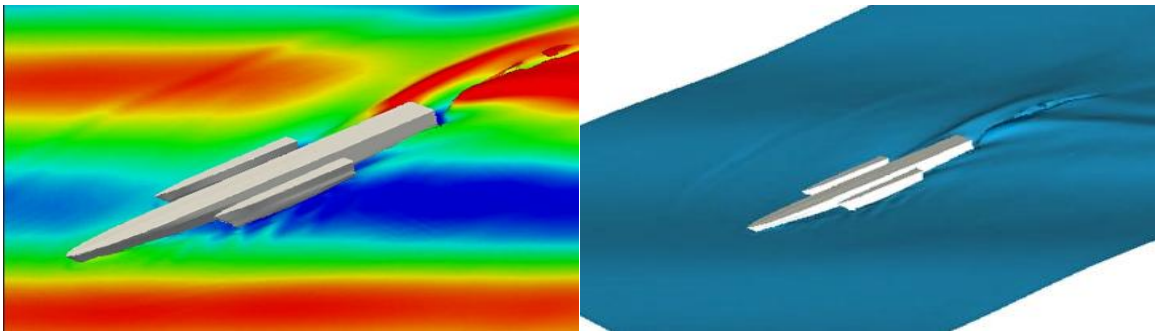
Fig. 11 The wave elevation of different layouts with broaching at Fr=0.45 (ak=0.096, β=30°, λ/L=1.1)



(a) The wave elevation of Layout 1



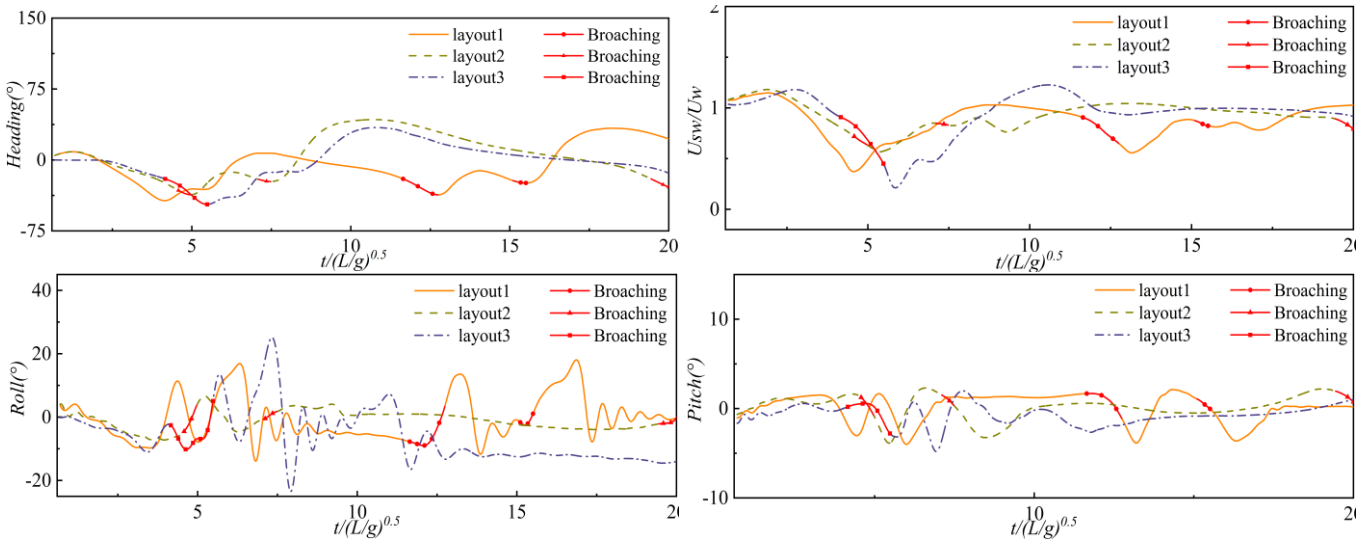
(b) The wave elevation of Layout 2



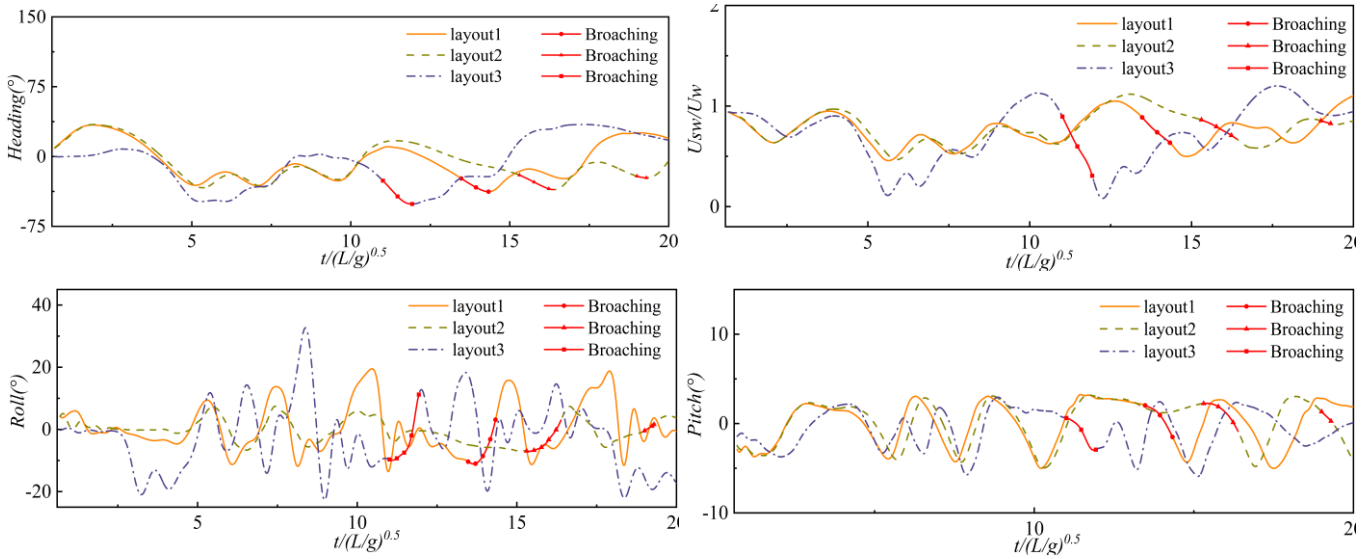
(c) The wave elevation of Layout 3

Fig. 12 The wave elevation of different layouts with broaching at Fr=0.55 (ak=0.096, β=30°, λ/L=1.1)

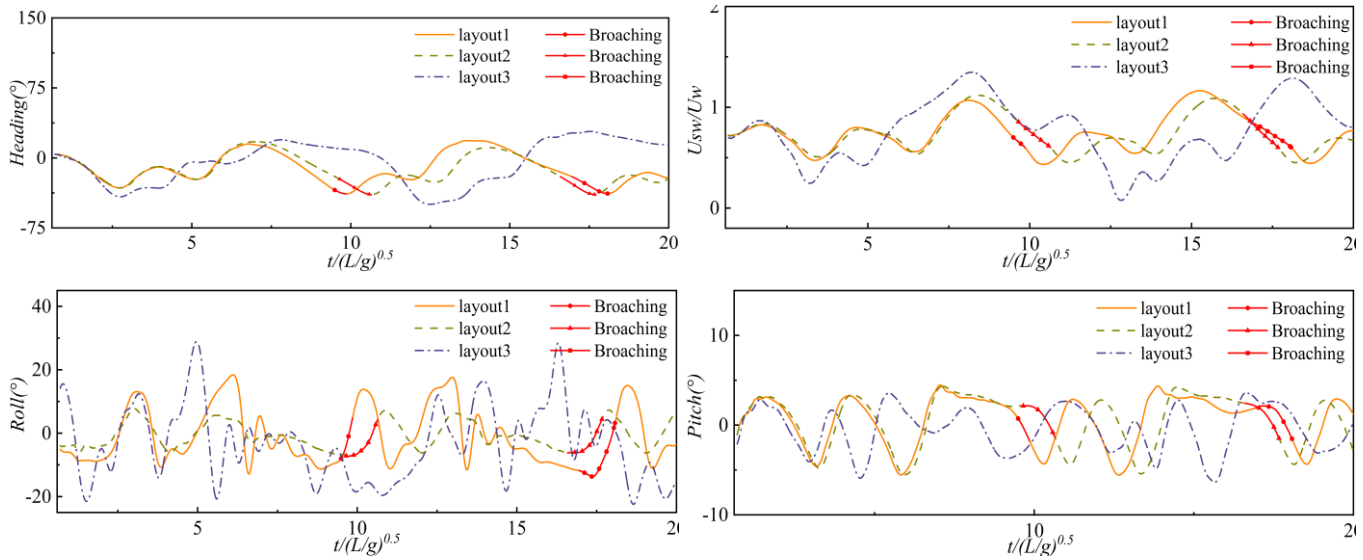
Figure 11 shows that at Fr=0.45, all three side-hull layouts have a tendency for broaching due to complex motion responses and unstable heading control. In Figure 12, the wave height contour plots at Fr=0.55 indicate that Layouts 1 and 2 have relatively stable wave propagation, higher stability and safety. Layout 3 experiences broaching, with wave distribution becoming notably asymmetrical and wave direction and intensity around the hull uneven.



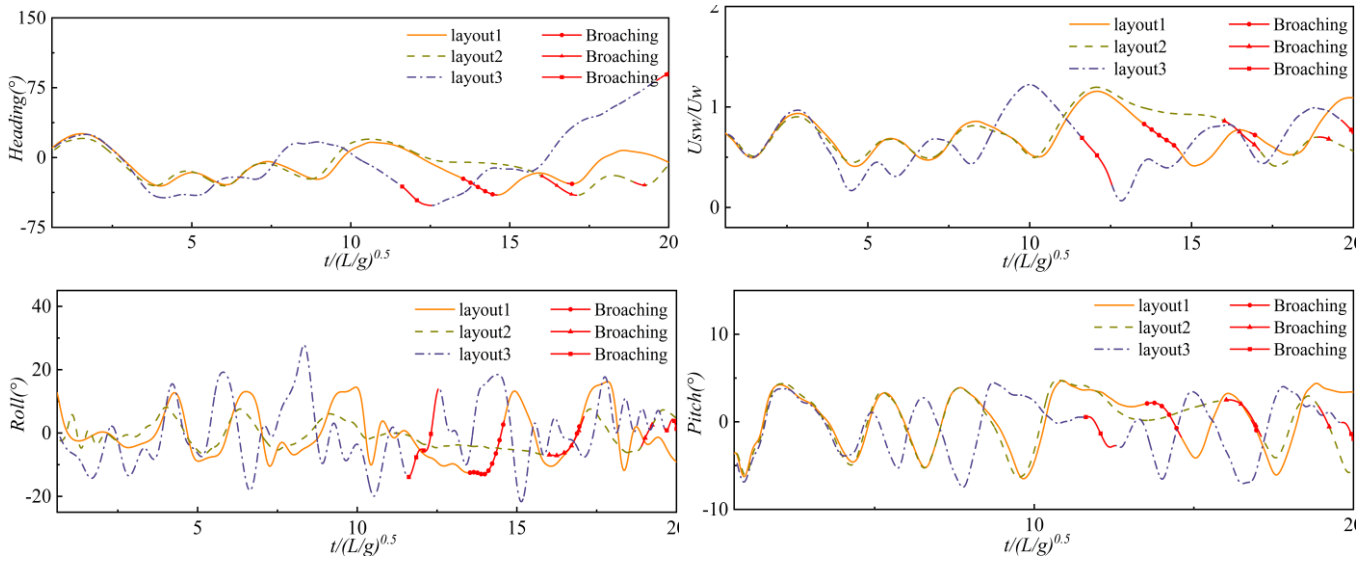
(a) heading, speed, roll and pitch motion (Fr=0.45, ak=0.140, β=30°, λ/L=0.9)



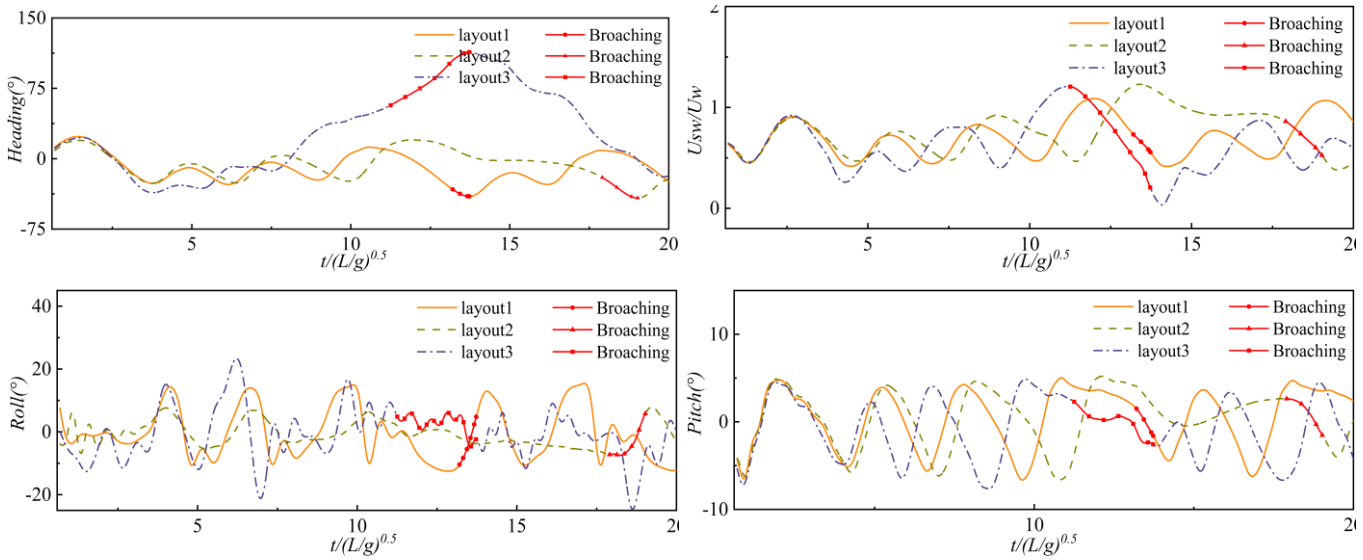
(b) heading, speed, roll and pitch motion (Fr=0.45, ak=0.140, β=30°, λ/L=1.1)



(c) heading, speed, roll and pitch motion (Fr=0.45, ak=0.140, β=30°, λ/L=1.3)



(d) heading, speed, roll and pitch motion (Fr=0.45, ak=0.140, β=30°, λ/L=1.5)



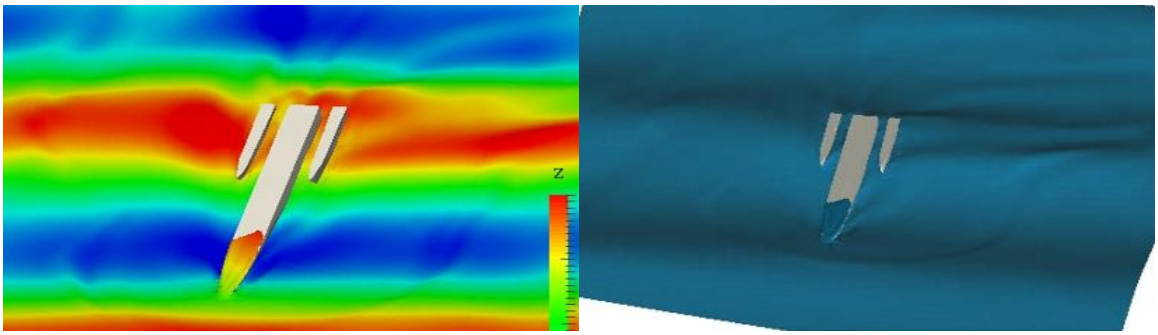
(e) heading, speed, roll and pitch motion (Fr=0.45, ak=0.140, β=30°, λ/L=1.7)

Fig. 13 The time history of computed results at various wavelength with broaching

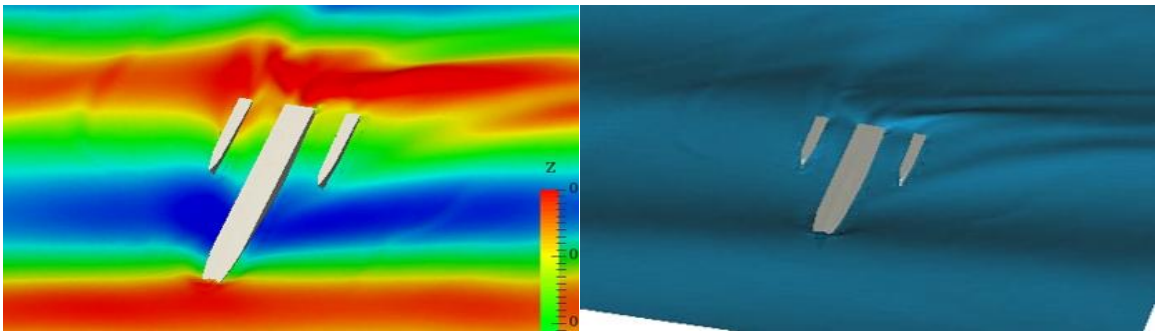
Figure 13 presents the time histories of heading angle, rudder angle, ship speed, roll and pitch for the three side-hull layouts at Fr=0.45, ak= 0.140 and β=30° with wavelength ratios λ/L= 0.9~1.7. The red solid lines denote the occurrence of broaching instability, respectively. As observed from Figure 13, at λ/L= 0.9, the heading deviation of Layout 1 is ±50°, which gradually narrows to±30° with increasing wavelength. The roll amplitude remains stable within ±15°, and the durations of broaching shorten as the wavelength increases. Layout 2 exhibits similar instability characteristics to Layout 1, with a roll amplitude ⩽10° and smaller heading deviation. Layout 3 exhibits the highest sensitivity to wavelength variations. Within the range of λ/L=0.9~1.5, its roll and pitch motion amplitudes are generally larger than those of Layouts 1 and 2, indicating a more pronounced tendency toward dynamic instability under most wavelength conditions. Under the condition of λ/L =1.5, the peak value of the heading deviation exceeds 100°, the roll amplitude is approximately 20°, and the broaching phenomenon occurs earlier compared with the other two schemes. When λ/L=1.7, the fluctuations in pitch, roll, and heading control are still significantly greater than those of Layouts 1 and 2; combined with the wave surface evolution results, it can be seen that the entire process is accompanied by severe bow wave overtopping and flow field disturbances. The roll curves show that Layout 2 achieves a significant roll reduction effect due to the increased transverse separation. In contrast, Layout 3

does not exhibit a roll reduction advantage and even shows increased roll in most cases. The forward shift of the side hulls in Layout 3 may result in higher sensitivity to short waves and larger oscillating amplitudes of roll and pitch. Compared with Layout 3, Layouts 1 and 2 exhibit smaller roll and pitch responses, indicating better motion stability. In comparison with the forward-shifted side-hull arrangement, Layouts 1 and 2 generally demonstrate weaker motion responses and a lower tendency toward dynamic instability under most wavelength conditions. In addition, their motion responses vary more moderately as the wavelength ratio increases. For Layout 3, the roll, pitch, and yaw responses are significantly greater than those of Layouts 1 and 2 within the range of $\lambda/L=0.9\sim1.5$, indicating that this configuration is more sensitive to wavelength variations. As the wavelength ratio increases, the motion responses generally become more pronounced, suggesting a stronger tendency toward dynamic instability. When the wavelength ratio further increases to $\lambda/L=1.7$, the ship's motion responses decrease to some extent, indicating a partial mitigation of the instability tendency. However, the motion responses of Layout 3 remain considerably larger than those of Layouts 1 and 2. In summary, under steep stern-quartering wave conditions, Layouts 1 and 2, which adopt an aft-positioned side-hull arrangement, exhibit smaller motion responses under most wavelength conditions. Their roll, pitch, and heading deviations are lower than those of Layout 3, indicating superior motion stability. Among the three configurations, Layout 2, with its larger transverse spacing between the side hulls and the main hull, demonstrates the most effective roll reduction and the lowest overall susceptibility to dynamic instability. This wavelength analysis was conducted under fixed initial Froude number, wave steepness, and incident wave heading angle. Therefore, the wavelength range associated with broaching identified in this study applies only to the present trimaran model and the other selected operating conditions and should not be regarded as a universal instability boundary. The coupling effects among initial speed, wave steepness, wavelength, incident wave heading angle, and initial wave phase have not yet been systematically investigated. In addition, the current results are based on regular-wave calculations, whereas irregular waves may lead to different probabilities of surfing and broaching, as well as different characteristics of the transition to instability.

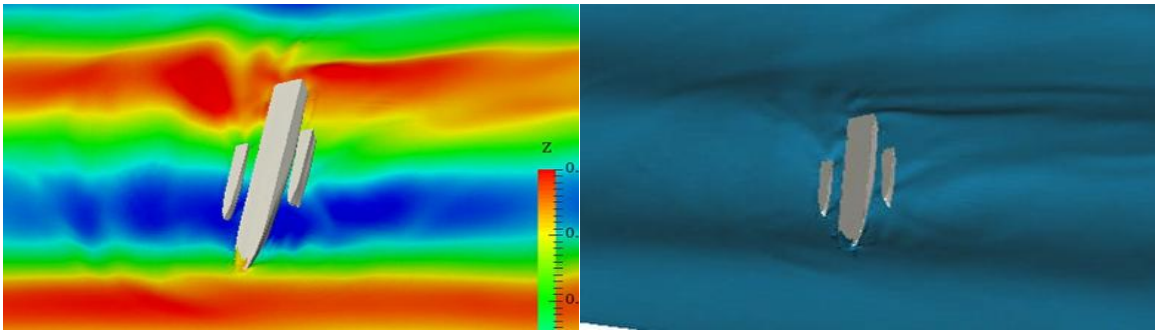
Figure 14 shows that, compared with other wavelength conditions, when $\lambda/L=1.3$, Layout 3 did not satisfy the broaching criterion, while Layouts 1 and 2 experienced broaching. Under this wavelength condition, all three layouts exhibited varying degrees of wave surface disturbance and deck wetness. This suggests that, at $\lambda/L = 1.3$, the hull design and side-hull arrangement of Layout 3 may help suppress broaching, making it potentially suitable for similar sea conditions.



(a) The wave elevation of Layout 1 (Fr=0.45, ak=0.140, β=30°, λ/L=1.3)



(b) The wave elevation of Layout 2 (Fr=0.45, ak=0.140, β=30°, λ/L=1.3)



(c) The wave elevation of Layout 3 (Fr=0.45, ak=0.140, β=30°, λ/L=1.3)

Fig. 14 The wave elevation of different layouts with broaching

5. Conclusion

A hybrid method is applied in this paper, coupling fully nonlinear potential flow theory with viscous flow theory. This method simulates broaching motion in quartering waves for a trimaran. The motion state of the trimaran is observed. The impact of initial speed is compared and analyzed. Different wave parameters and various side-hull configurations are also examined. They affect the trimaran's behavior in following and quartering waves. A preliminary assessment is made of the trimaran's sailing characteristics under different side-hull configurations. The main conclusions of this study are as follows.

(1) Layout 3, with forward-side hulls, is the most sensitive to speed and pitch variations. It shows strong coupling between heading and roll angles and pronounced nonlinear motion. In contrast, Layouts 1 and 2, with stern-side hulls, maintain more uniform pressure distribution and better course-keeping ability. The improved stability of Layout 2 is mainly attributed to the increased transverse separation, which reduces hydrodynamic interference between the main hull and side hulls, weakens cross-wave impacts, and enhances effective rudder force. The waterjet propulsion system responds differently to heading deviations and roll motions under different layouts, which further affects heading control authority and instantaneous acceleration during broaching.

(2) Broaching characteristics of a trimaran in following seas are significantly affected by the layout of its outriggers. Forward-mounted outriggers significantly increase the risk of broaching, leading to earlier

occurrence, longer duration, and more severe heading loss. Aft-mounted outriggers effectively suppress broaching, and the configuration with increased transverse separation exhibits the optimal anti-broaching performance. Increased wave steepness and high-risk wave wavelengths significantly intensify broaching. By stabilizing the flow field, enhancing directional damping, and improving steering efficiency, aft-mounted outriggers significantly improve the anti-broaching capability and navigation safety of a trimaran in following seas.

(3) Among the three different layout schemes, Layout 1 exhibits favorable stability under moderate and low sea conditions, effectively avoiding broaching behaviors with smooth pitch motion. However, its anti-broaching capability is relatively limited, and its roll amplitude and heading deviation under high wave steepness conditions are both larger than those of Layout 2. Layout 2 is the optimal scheme with the best overall performance. It demonstrates the highest navigation stability under all working conditions, featuring the minimum roll amplitude, the best course-keeping ability, and the lowest wave-induced resistance occurrence. It can significantly suppress broaching, with its roll amplitude reduced by approximately 50 % compared with Layout 3. Layout 3 has the poorest overall stability. Its roll amplitude can reach 1.3 to 2 times that of Layout 1 and Layout 2, and the heading deviation increases by about 233 %. It is more prone to early broaching, with the instability speed advanced by 15.6 % and the unstable wavelength range expanded by 60 % to 80 %. It only has a slight advantage in pitch amplitude.

Although the hybrid numerical method employed in this study has been validated via grid convergence analysis, the main limitation of the algorithm lies in the simplified waterjet propulsion model, which cannot fully represent the actual waterjet propulsion system and neglects the influences of waves and large-amplitude motions on propulsion efficiency. Meanwhile, the method is limited by the FNPT+CFD coupling assumption, the regular wave model, the selection of three typical layout schemes, and fixed PD control parameters, without considering irregular waves, fluid-structure interaction effects, and operational differences of real ships. Future research can carry out numerical simulations under irregular wave conditions, model tests, and multi-objective layout optimization studies. In addition, the mechanism of how the waterjet propulsion system affects broaching during the broaching process will also be one of the key focuses of subsequent research. Furthermore, this study did not establish a complete threshold or probability of occurrence for wave riding. Several deterministic cases were selected to examine the effects of initial velocity and wave conditions, rather than conducting a systematic multidimensional parametric study. The predicted instability may also be related to the initial wave phase, the initial position of the vessel, initial motion disturbances, and the selected autopilot parameters. Therefore, the critical velocity and wavelength ranges given in the paper can only be regarded as results obtained under specific conditions for the current trimaran model and cannot serve as general criteria for determination. Future studies should include repeated simulations under different initial phases, systematic parameter sweeps over velocity-wave conditions, irregular wave simulations, and experimental validation.

FUNDING

This project was supported by the National Natural Science Foundation of China (Grant number 52401385), Open Research Project of State Key Laboratory of Maritime Technology and Safety (Grant number W25CG000073), and MTIC-JUST Joint Innovation Center Development Fund.

REFERENCES

[1] IMO. Interim Guidelines on the Second Generation Intact Stability Criteria. Circular MSC.1/1627, *International Maritime Organization*, London, UK, 2020.

[2] Nazemian, A. and Ghadimi, P., 2021. Global optimization of trimaran hull form to get minimum resistance by slender body method. *Journal of the Brazilian Society of Mechanical Sciences and Engineering*, 43, 67. https://doi.org/10.1007/s40430-020-02791-8

[3] Yildiz, B., Sener, B., Duman, S., Datla, R. 2020. A numerical and experimental study on the outrigger positioning of a trimaran hull in terms of resistance. *Ocean Engineering*, 198, 106938. https://doi.org/10.1016/j.oceaneng.2020.106938

[4] Guo, J., Chen, Z., Dai, Y. 2020. Numerical study on self-propulsion of a waterjet propelled trimaran. *Ocean Engineering*, 195, 106655. https://doi.org/10.1016/j.oceaneng.2019.106655

[5] Guo, J., Zhang, Y., Chen, Z., Feng, Y., 2020. CFD-based multi-objective optimization of a waterjet-propelled trimaran. *Ocean Engineering*, 195, 106755. https://doi.org/10.1016/j.oceaneng.2019.106755

[6] Gong, J., Li, Y., Jiang, F., Hong, Z., Yu, D., 2020. Maneuvering simulation and study on the effect of hull attitude on maneuverability of trimarans by OpenFOAM. *Journal of Coastal Research*, 36(1), 157-173. https://doi.org/10.2112/JCOASTRES-D-19-00086.1

[7] Jiang, F., Li, Y., Gong, J., 2021. Study on the manoeuvre characteristics of a trimaran under different layouts by water-jet self-propulsion model test. *Applied Ocean Research*, 108, 102550. https://doi.org/10.1016/j.apor.2021.102550

[8] Li, Y., Tang, Z., Gong, J., 2023. The effect of PID control scheme on the course-keeping of ship in oblique stern waves. *Brodogradnja*, 74(4), 155-178. https://doi.org/10.21278/brod74408

[9] Li, A., Li, Y., Zhang, D., Fu, Z., 2020. Numerical study on hydrodynamic coefficients and longitudinal motions of trimaran in head seas for various wave slopes. *Journal of the Brazilian Society of Mechanical Sciences and Engineering*, 42(4), 186. https://doi.org/10.1007/s40430-020-02286-6

[10] Nowruzi, L., Enshaei, H., Lavroff, J., Davis, M.R., 2020. Parametric study of seakeeping of a trimaran in regular oblique waves. *Ships and Offshore Structures*, 15(Suppl. 1), S98-S109. https://doi.org/10.1080/17445302.2020.1735809

[11] Begovic, E., Gatin, I., Jasak, H., Rinauro, B., 2020. CFD simulations for surf-riding occurrence assessment. *Ocean Engineering*, 218, 107975. https://doi.org/10.1016/j.oceaneng.2020.107975

[12] Gong, J., Li, Y., Yan, S., Ma, Q., 2022. Numerical simulation of turn and zigzag maneuvres of trimaran in calm water and waves by a hybrid method. *Ocean Engineering*, 253, 111239. https://doi.org/10.1016/j.oceaneng.2022.111239

[13] Gong, J., Li, Y., Cui, M., Yan, S., Ma, Q., 2022. Study on the surf-riding and broaching of trimaran in oblique stern waves. *Ocean Engineering*, 266, 112995. https://doi.org/10.1016/j.oceaneng.2022.112995

[14] Liang, L., Baoji, Z., Hao, Z., Jiaye, G., Zhang, T., Shuhui, G., Yuanbiao, B., Xu, Z., 2024. Study on numerical simulation and mitigation of parametric rolling in a container ship under head waves. *Brodogradnja*, 2024, 75(3), 75305. https://doi.org/10.21278/brod75305

[15] Liu, L., Yao, C., Feng, D., Wang, X., Yu, J., Chen, M., 2022. Numerical study of the interaction between the pure loss of stability, surf-riding, and broaching on ship capsizing. *Ocean Engineering*, 2022, 266, 112868. https://doi.org/10.1016/j.oceaneng.2022.112868

[16] Ma, C., Ma, N., Gu, X., Feng, P., 2021. Numerical study on hydrodynamic forces and course stability of a ship in surf-riding condition based on planar motion mechanism tests. *Journal of Offshore Mechanics and Arctic Engineering*, 143(6), 061901. https://doi.org/10.1115/1.4051152

[17] Zhou, B., Wu, Z., Lin, X., Yi, W., Liu, H., Zhang, G., 2025. Numerical study on hydrodynamic performance of a trimaran in regular waves considering steady flow and shallow water effects. *Ocean Engineering*, 330, 121103. https://doi.org/10.1016/j.oceaneng.2025.121103

[18] Jeong, S.-M. and Park, S., 2025. Dynamic stability and safety of ships in waves. *Journal of Marine Science and Engineering*, 2025, 13(10), 1950. https://doi.org/10.3390/jmse13101950

[19] Rusche, H., 2002. Computational fluid dynamics of dispersed two-phase flows at high phase fractions. *Imperial College*, London, UK.

[20] Weller, H.G., 2002. Derivation, modelling and solution of the conditionally averaged two-phase flow equations. Technical Report TR/HGW/02, *Nabla Ltd.*

[21] Gong, J., Li, Y., Cui, M., Fu, Z., Zhang, D., 2021. The effect of side-hull position on the seakeeping performance of a trimaran at various headings. *Ocean Engineering*, 239, 109897. https://doi.org/10.1016/j.oceaneng.2021.109897

[22] Hu, Z., Yan, S., Greaves, D., Mai, T., Raby, A., Ma, Q., 2020. Investigation of interaction between extreme waves and a moored FPSO using FNPT and CFD solvers. *Ocean Engineering*, 206, 107353. https://doi.org/10.1016/j.oceaneng.2020.107353

[23] Ma, Q. and Yan, S., 2009. QALE-FEM for numerical modelling of non-linear interaction between 3D moored floating bodies and steep waves. *International Journal for Numerical Methods in Engineering*, 78(6), 713-756. https://doi.org/10.1002/nme.2505

[24] Yan S. and Ma Q., 2010. QALE-FEM for modelling 3D overturning waves. *International Journal for Numerical Methods in Fluids*, 63, 743-768. https://doi.org/10.1002/fld.2100

[25] Dai, K., Li, Y., Gong, J., Fu, Z., Li, A., Zhang, D., 2022. Numerical study on propulsion factors in regular head and oblique waves. *Brodogradnja*, 73(1), 37-56. https://doi.org/10.21278/brod73103

[26] Dai K. and Li Y., 2021. Experimental and numerical investigation on maneuvering performance of small waterplane area twin hull. *Brodogradnja*, 72(2), 93-114. https://doi.org/10.21278/brod72206

[27] Jong, P., Renilson, M., Walree, F., 2013. The broaching of a fast rescue craft in following seas. *Proceedings of the 12th International Conference on Fast Sea Transportation*, 2-5 December, Amsterdam, Netherlands.

[28] Umeda, N., Araki, M., Hashimoto, H., 2008. Numerical simulation on dynamic behavior of a trimaran running in following and quartering waves. *Proceedings of the 3rd Pan Asian Association of Maritime Engineering Societies* (PAAMES) *and Advanced Maritime Engineering Conference* (AMEC2008), China, 2008, 197-203.

[29] Gong, J., Li, Y., Fu, Z., Li, R., Hong, Z., 2022. Study on the characteristics of trimaran's surf-riding in stern waves by a hybrid method. *Ocean Engineering*, 265, 112603. https://doi.org/10.1016/j.oceaneng.2022.112603

[30] Gong J., Li Y., Dai K., Fu, Z., Hong, Z., 2022. Numerical simulation of ship maneuvring by a hybrid method with propulsive factors in waves taken into account. *Ocean Engineering,* 264, 112538. https://doi.org/10.1016/j.oceaneng.2022.112538

[31] Yan, S., Wang, J., Wang, J., Ma, Q., Xie, Z., 2019. Numerical simulation of wave structure interaction using QaleFOAM. *Proceedings of the 29th International Offshore and Polar Engineering Conference*, 16-21 June, Honolulu, Hawaii, USA.

[32] ITTC Recommended Procedures and Guidelines, 2017. Uncertainty analysis in CFD verification and validation-methodology and validation 7.5-03-01-01. *Proceedings of the 28th International Towing Tank Conference*.

[33] Fossati, F., 2009. Aero-hydrodynamics and the performance of sailing yachts: the science behind sailing yachts and their design. *A&C Black*.

[34] Umeda, N. and Hashimoto, H., 2002. Qualitative aspects of nonlinear ship motions in following and quartering seas with high forward velocity. *Journal of Marine Science and Technology*, 6(3), 111-121. https://doi.org/10.1007/s007730200000

[35] Ghadimi, P., Nazemian, A., Sheikholeslami, M., 2019. Numerical simulation of the slamming phenomenon of a wave-piercing trimaran in the presence of irregular waves under various seagoing modes. *Journal of Engineering for the Maritime Environment*, 233(4), 1198-1211. https://doi.org/10.1177/1475090218819186

[36] Maki, A., Umeda, N., Renilson, M., Ueta, T., 2014. Analytical methods to predict the surf riding threshold and the wave-blocking threshold in astern seas. *Journal of Marine Science and Technology*, 19, 415-424. https://doi.org/10.1007/s00773-014-0257-2

[37] Maki, A., Umeda, N., Renilson, M., Ueta, T., 2010. Analytical formulae to predict the surf riding threshold for a ship in following waves. *Journal of Marine Science and Technology*, 15, 218-229. https://doi.org/10.1007/s00773-010-0085-y

[38] Faltinsen, O., 1993. Sea loads on ships and offshore structures. *Cambridge University Press*. https://doi.org/10.4043/7142-MS

[39] Ogilvie, T., 1964. Recent progress toward the understanding and prediction of ship motions. *Proceedings of the Fifth Symposium on Naval Hydrodynamics*, 10-12 September, Bergen, Norway, 3-79.